AD-A150 350 TIME-RESOLVED REFLECTIVITY MEASUREMENT OF EXTRINSIC SILICON DURING PULSED LASER IRRADIATION(U) NAVAL POSTGRADUATE SCHOOL MONTEREY CA G D JOHNSON ET AL. 1/2

UNCLASSIFIED JUN 84 F/G 20/6 NL

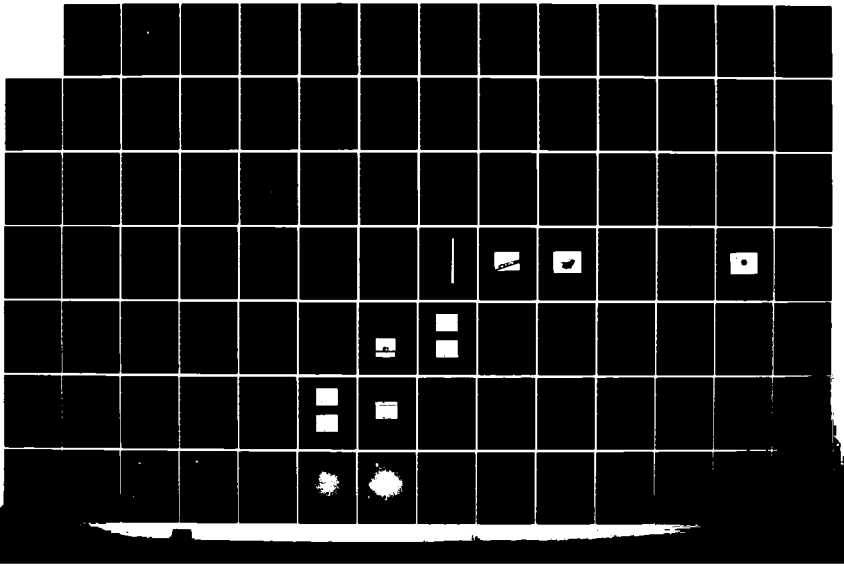

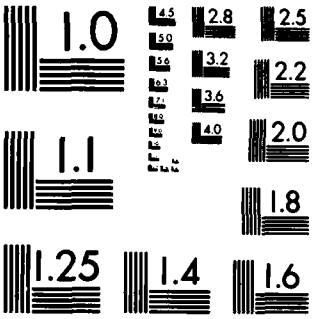

(2)

NAVAL POSTGRADUATE SCHOOL
Monterey, California

THESIS

TIME-RESOLVED REFLECTIVITY MEASUREMENT OF EXTRINSIC SILICON DURING PULSED LASER IRRADIATION

by

Geoffrey Davis Johnson
and
Emory Leigh Chenoweth

June 1984

Thesis Advisor: A.W. Cooper

SECURITY CLASSIFICATION OF THIS PAGE (When Data Entered)

REPORT DOCUMENTATION PAGE		READ INSTRUCTIONS BEFORE COMPLETING FORM
1. REPORT NUMBER	2. GOVT ACCESSION NO. A150350	3. RECIPIENT'S CATALOG NUMBER
4. TITLE (and Subtitle) Time-Resolved Reflectivity Measurement of Extrinsic Silicon During Pulsed Laser Irradiation		5. TYPE OF REPORT & PERIOD COVERED Master's Thesis; June 1984 6. PERFORMING ORG. REPORT NUMBER
7. AUTHOR(s) Geoffrey Davis Johnson and Emory Leigh Chenoweth		8. CONTRACT OR GRANT NUMBER(s)
9. PERFORMING ORGANIZATION NAME AND ADDRESS Naval Postgraduate School Monterey, California 93943		10. PROGRAM ELEMENT, PROJECT, TASK AREA & WORK UNIT NUMBERS
11. CONTROLLING OFFICE NAME AND ADDRESS Naval Postgraduate School Monterey, California 93943		12. REPORT DATE June 1984 13. NUMBER OF PAGES 99
14. MONITORING AGENCY NAME & ADDRESS(if different from Controlling Office)		15. SECURITY CLASS. (of this report) Unclassified 15a. DECLASSIFICATION/ DOWNGRADING SCHEDULE

16. DISTRIBUTION STATEMENT (of this Report)

Approved for public release; distribution unlimited

17. DISTRIBUTION STATEMENT (of the abstract entered in Block 20, if different from Report)

18. SUPPLEMENTARY NOTES

19. KEY WORDS (Continue on reverse side if necessary and identify by block number)
Time Resolved Reflectivity, Extrinsic Silicon, Laser-Induced Damage, Melting Threshold, Damage Threshold

20. ABSTRACT (Continue on reverse side if necessary and identify by block number)
Time-resolved reflectivity (TRR) of crystalline silicon has been measured with nanosecond resolution during and immediately after pulsed neodymium:glass laser irradiation (1.06 μm, full width at half maximum pulse duration of 20 ns) over a range of pulsed laser energy densities. The TRR information was used to determine energy density thresholds for melting and damaging the polished surface of extrinsic silicon wafers. Reflectivity initially increased under laser irradiation and then returned to its original value for energy densities between

DD FORM 1 JAN 73 1473 EDITION OF 1 NOV 65 IS OBSOLETE
S/N 0102-LF-014-6601

SECURITY CLASSIFICATION OF THIS PAGE (When Data Entered)

20. (Continued)

0.46 J/cm^2 and 1.05 J/cm^2. For energy densities greater than 1.05 J/cm^2, the final value of reflectivity was less than the original value due to permanent target damage. The damage threshold was substantiated with optical photomicrographs. A qualitative examination was undertaken to determine the change in specular and diffuse reflection from the target surface as a function of the degree of laser-induced damage.

Approved for publ release; distribution unlimited

Time-Resolved Reflectivity Measurement of Extrinsic Silicon During Pulsed Laser Irradiation

by

Geoffrey Davis Johnson
Lieutenant, United States Navy
B.S., North Carolina State University, 1977

and

Emory Leigh Chenoweth
Lieutenant, United States Navy
B.S., United States Naval Academy, 1976

Submitted in partial fulfillment of the requirements for the degree of

MASTER OF SCIENCE IN PHYSICS

from the

NAVAL POSTGRADUATE SCHOOL
June 1984

Author: Geoff D Johnson

Author: Emory L Chenoweth

Approved by: R W Cooper
Thesis Advisor

John R Neighbours
Second Reader

Y Le Schacher
Chairman, Department of Physics

J M Dyer
Dean of Science and Engineering

ABSTRACT

Time-resolved reflectivity (TRR) of crystalline silicon has been measured with nanosecond resolution during and immediately after pulsed neodymium:glass laser irradiation (1.06 μm, full width at half maximum pulse duration of 20 ns) over a range of pulsed laser energy densities. The TRR information was used to determine energy density thresholds for melting and damaging the polished surface of extrinsic silicon wafers. Reflectivity initially increased under laser irradiation and then returned to its original value for energy densities between 0.46 J/cm^2 and 1.05 J/cm^2. For energy densities greater than 1.05 J/cm^2, the final value of reflectivity was less than the original value due to permanent target damage. The damage threshold was substantiated with optical photomicrographs. A qualitative examination was undertaken to determine the change in specular and diffuse reflection from the target surface as a function of the degree of laser-induced damage.

TABLE OF CONTENTS

I. INTRODUCTION

The field of electro-optics (EO) has experienced phenomenal growth in the past decade and with this expansion there has been a concomitant military effort to apply the results of electro-optical research to weapons development. One needs only examine the pages of JANES Weapons Systems 1983-84 [Ref. 1] to view the proliferation of electro-optical and infrared (IR) sensing systems in the arsenals of the world's militaries. The deployment and utilization of EO warfare devices upon the battlefields of the future are assured. Advances in the rapidly developing, solid-state detector technology have spawned a new generation of highly sensitive electronic components designed to effectively exploit the visible and infrared portions of the electromagnetic spectrum. Applications ranging from IR homing and EO guided missiles and munitions to night vision devices and IR scanners/trackers are present-day tactical realities which dictate the need for reliable countermeasures (CM). The diverse nature of the threat would seem to preclude any single system as a viable EO countermeasure. Yet one device has demonstrated the capability to effectively neutralize a wide range of EO sensors and components. This device is the laser.

A high intensity, coherent, and potentially high energy source of electromagnetic radiation, the laser is destined to play an important role in EO countermeasures. "Widespread deployment of laser countermeasures for self-protection of battlefield assets could deprive the enemy of some of his most accurate weapons. The laser CM mechanism will vary from simple image blooming which temporarily blinds the optical system to saturation which could be relatively long term but not permanent, to permanent damage of elements in the EO devices" [Ref. 2]. Designed to operate within a limited range of system parameters, EO detectors will experience a serious degradation in their performance and reliability as a result of laser-induced variations of the photo-sensitive elements' optical and electrical properties.

Elemental semiconductors, such as silicon and germanium, are among the technologically most important materials for the manufacture of solid-state detectors. As characterized by the RCA Electro-Optics Handbook, "The silicon photo-detector is small, reliable, and has high quantum efficiency through the visible to near infrared" [Ref. 3]. It is due to these factors that silicon detectors have been incorporated into a wide range of military EO systems. Because of its prevalence in current EO devices and commercial availability, silicon was chosen as the target material.

In this research, time-resolved measurements were made of the reflectivity of p-type silicon under the influence of pulsed laser radiation. These results along with the examination of the irradiated samples by optical microscopy may help determine the laser energy density thresholds for variation of the target's optical properties and the onset of permanent surface damage. Certain aspects of this research evolved from parallel studies of pulsed laser annealing of semiconductors. Where possible, qualitative comparisons were made between the results of earlier experiments and the findings of these investigations in the variations of time-resolved optical properties of semiconductors. Also, investigation of probe laser beam scattering was conducted in an attempt to relate the specular versus diffuse components of reflectivity and the degree of laser-induced target surface damage.

II. BACKGROUND

A. INTRODUCTION

This investigation of the effect of pulsed laser radiation upon the time-resolved reflectivity (TRR) of extrinsic silicon was an outgrowth of research in laser-target damage conducted over the past decade at the Naval Postgraduate School. Studies elsewhere concerning laser radiation effects in semiconductors have been pursued for a myriad of purposes and have observed a variety of physical and electrical properties. The promise held by pulsed laser annealing in the processing of device-grade semiconductor material and the application of laser technology as a countermeasure to military EO systems are two motivations which continue to generate considerable scientific interest and research. Preparatory to a synopsis of previous work accomplished in the area of laser interaction with semiconductors, a brief review will be undertaken covering the phenomenon of photoconductivity, the photovoltaic effect, and an examination of the operation of several classes of photodetectors which utilize extrinsic silicon will be conducted. Detailed treatments of the band theory of semiconductors and the physics of photoconductive and photovoltaic devices can be found in many competent texts

[Refs. 4, 5, 6]. The intention here is only to present the basic mechanisms and give a fundamental understanding of photoconductivity and the photovoltaic effect in semiconductors so as better to understand the problem of pulsed laser irradiation of these materials.

B. PHOTOCONDUCTIVITY IN SEMICONDUCTORS

The use of the photoconductive effect for optical radiation detectors utilizes the change in resistance of a semiconductor caused by photon absorption and consequent hole-electron pair generation. Two specific sub-categories of photoconductive detection exist, classified by the nature of the photo-excitation. In the first of these categories, intrinsic excitation, hole-electron pairs are generated in the pure semiconductor material when photons with energy greater than the bandgap are absorbed, thereby exciting an electron from the valence band to the conduction band. It follows that the value of the bandgap sets an effective limit to the wavelength of radiation which may be detected by a photoconductive detector employing an intrinsic semiconductor. As an example, the energy bandgap in pure silicon is 1.09 eV which corresponds to a wavelength detection limit of approximately 1.14 μm, or less (i.e., $\lambda_c < 1.09$ eV/(hc) where h is Planck's constant and c is the speed of light). To broaden the spectral response of intrinsic semiconductors, impurities are introduced into the

lattice structure. Depending upon the atomic species of the dopant material, radiation incident upon an extrinsic, or doped, semiconductor might excite a donor, creating an excess electron in the conduction band for an n-type semiconductor or an excess hole in the valence band by promoting an electron to an acceptor level in a p-type material [Ref. 7]. Figure 1 depicts the process of photoconduction in intrinsic and extrinsic semiconductors.

There exists a wide range of dopants which may be used as impurities in the semiconductor lattice. Each atomic species has its own value of photo-activation energy and consequently extrinsic semiconductors can be fashioned into detectors capable of operating over a range of wavelengths. The activation energy is the single most important property of the impurity in controlling wavelength response of the detector. For the militarily significant three to five μm and eight to fourteen μm spectral bands, the appropriate activation energies are approximately 0.25 eV and 0.09 eV. The most commonly selected impurities for implantation in silicon to effect optical detection in the eight to fourteen μm band are arsenic, aluminum, gallium, bismuth, and magnesium with respective activation energies of 0.054, 0.068, 0.071, 0.072, and 0.107 ev [Refs. 8, 9]. These relatively small values of energy required for photo-excitation give rise to the most significant problem

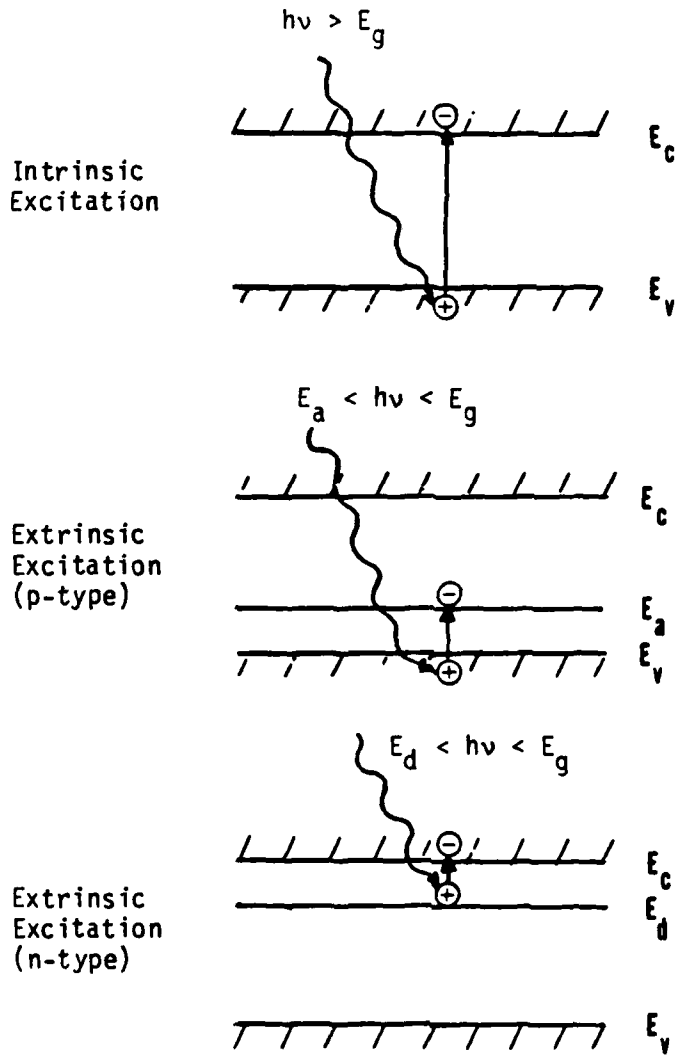

Figure 1. Photoconductive Processes in Semiconductors (where the bandgap energy, $E_g = E_c - E_v$)

associated with photodetection of longer wavelength radiation. In order to ensure that the impurities are not subjected to thermal excitation which would mask the optical excitation, the detector must be cooled to low operating temperatures.

C. PHOTOVOLTAIC EFFECT IN SEMICONDUCTORS, THE P-N JUNCTION

Semiconductor p-n junction photodiodes are widely utilized for optical detection of wavelengths in the visible and IR spectrum. A p-n junction is a single crystal of semiconducting material in which part of the material is p-type and part is n-type. The spatial change from p-type material to n-type material at the junction is abrupt.

In operation, the junction of the photodiode is usually reverse-biased (the positive terminal of an external voltage source is connected to the n-type material), with the battery and photodiode connected in series with an external load resistor, as shown in Figure 2. With no photon flux incident on the photodiode, the junction is in equilibrium, and no current flows in the external circuit. When the junction is illuminated, charge carriers in the form of free electrons and holes are created as depicted in Figure 3. The movement of the holes and electrons to establish the back-biased equilibrium creates a current in the circuit, providing an electrical signal to indicate that radiation has been detected. For high sensitivity, one can produce a

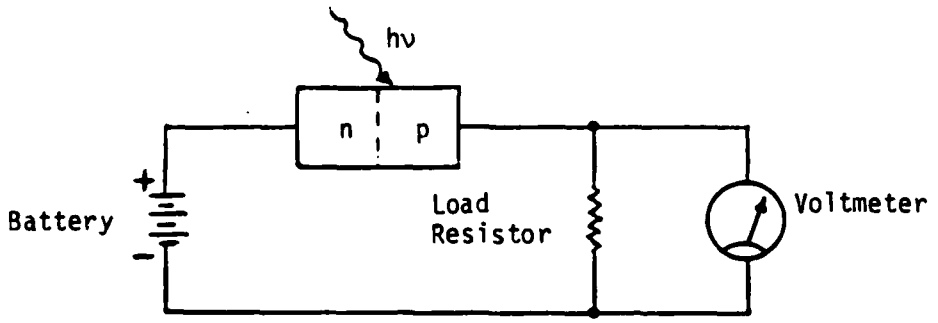

Figure 2. Construction of a p-n Junction Photodiode Detector (Reverse-Biased)

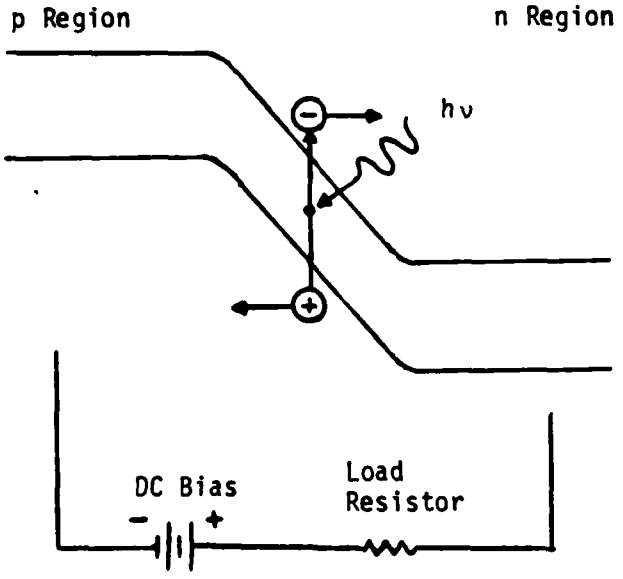

Figure 3. Electron-Hole Pair Creation by an Absorbed Photon that Contributes to Current Flow in a p-n Photodiode

device with a large junction volume by sandwiching an intrinsic semiconductor between the n-type and p-type regions. Such a device is known as a p-i-n photodiode [Refs. 10, 11].

D. EXTRINSIC SILICON PHOTODETECTORS

Having established the basic physical mechanisms underlying the phenomena of photoconductivity and the photovoltaic effect in semiconductors, specific devices and components based upon silicon and operating by these two processes will now be surveyed. This examination is in no way deemed to be complete in its scope, but rather it is intended as a limited overview of current applications of silicon detector technology.

Concentrating first upon the visible and near IR portion of the electromagnetic spectrum, imaging and camera tubes have long employed silicon as a photoconductive target for light sensing. Perhaps the most widely used type of camera tube is the vidicon. The vidicon utilizes an electron beam to scan a photoconductive target which is the light sensor. A transparent conductive layer applied to the front side of the photoconductor serves as the signal electrode. In operation, the scanning beam initially charges the back side of the target to cathode potential. When a light pattern is focused on the photoconductor, its conductivity increases in the illuminated areas and the back side of the target

charges to more positive values. The electron beam then reads the signal by depositing electrons on the positively charged areas thereby providing a capacitively coupled signal at the signal electrode. A schematic rendering of a vidicon tube is presented in Figure 4 [Ref. 12]. The reliability and ruggedness of the vidicon tube has made it the leading choice for current television systems in military appreciations. This type of tube, however, does exhibit a problem with regard to the overload characteristic of the target. If the image of a very intense radiation source in the scene discharges the diodes of a silicon diode array target in a time much shorter than a frame time, the resulting white spot in the reproduced image often appears many times larger than the radiation image should [Ref. 13]. Image blooming such as that described here will potentially degrade the vidicon for a period of time longer than the period of illumination. Should the energy density of the radiation be sufficiently high, the vidicon's photoconductive target may be permanently damaged.

Shifting focus to the middle and far IR portion of the spectrum, extrinsic silicon infrared charge coupled devices (IRCCD) are the central issue in development of imaging systems. The primary distinction between the IRCCD and other solid state imaging sensors is in the readout process. In the IRCCD, the collected charge is scanned out by

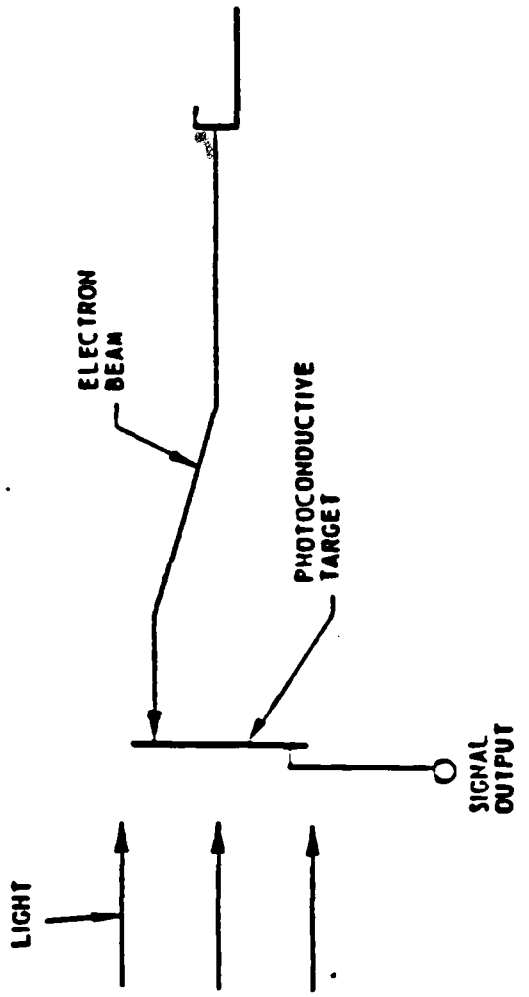

Figure 4. Schematic Diagram of a Typical Vidicon Imaging Tube

sequencing the phased electrode voltages that establish the electric field potential wells within the silicon. In this fashion the charge in a given well can be moved laterally from well to well and out to a charge sensitive amplifier built into the same silicon wafer. In surface channel IRCCDs the potential well is at the interface of the silicon and silicon dioxide insulating layer. Imperfections at this interface result in charge trapping which seriously degrades the performance at low signal levels. Using CCD and photodiode array techniques for multiplexing and signal processing, it has become practical to make IR focal planes with thousands of IR detectors. In one monolithic extrinsic silicon IRCCD array, gallium doped silicon is utilized for development of a forward-looking infrared system covering the eight to fourteen m band [Ref. 14]. The production and testing of new devices based upon the IRCCD technology is well documented in the open literature [Refs. 15, 16, 17, 18]. Figure 5 shows the construction of a monolithic silicon IRCCD.

E. THEORY: MODELS OF OPTICAL HEATING IN SEMICONDUCTORS

Having examined the means by which extrinsic semiconductors operate and devices in which the materials are employed, it now remains to investigate the models which attempt to explain the effects of laser energy deposition upon such semiconductors. It is apparent that thresholds

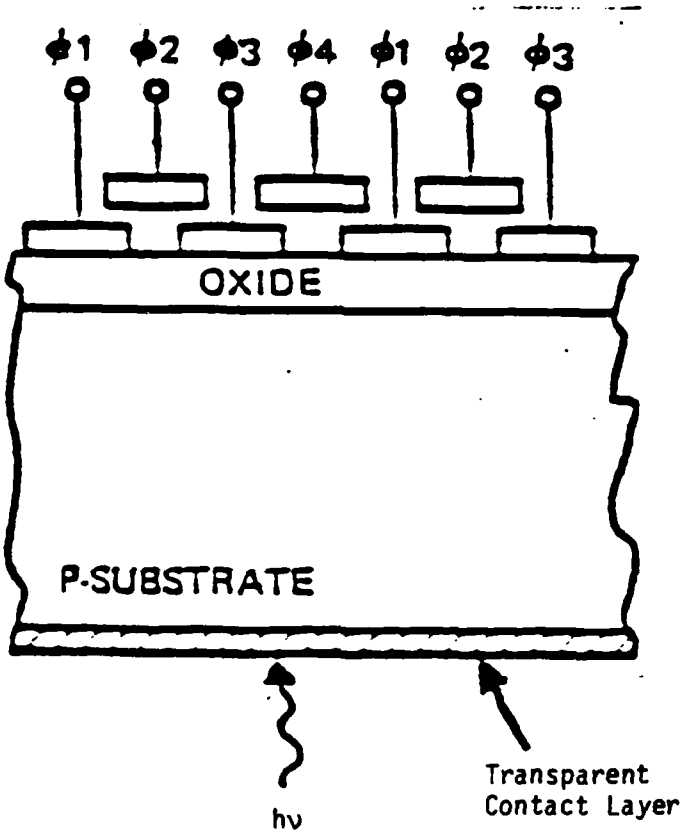

Figure 5. Typical Construction of an Extrinsic Silicon IRCCD

for damage in these substances depend on a variety of factors related to both the properties of the substance itself and the characteristics of the laser radiation. To obtain a model which would accurately predict damage thresholds while accounting for these many variables would be a vast and exceedingly complex undertaking.

As a first and simple approach, the interaction of a laser beam with an extrinsic semiconductor can be described in terms of energy transfer from the photon to the phonon field. The absorbed laser photons generate electron-hole pairs, which recombine by nonradiative transitions and serve to transfer energy to the lattice. A version of the heat diffusion equation, including a source term to account for absorption, serves as a useful tool to model the laser-semiconductor interaction. Many variants of the equation have been proposed [Refs. 19, 20, 21] but the form which provides adequate correlation with experimental data and a lesser degree of mathematical complexity assumes a laser beam intensity uniform in cross-section. This simplification reduces the problem to a one dimensional case, where the physical quantities are dependent only upon the variables of time and distance from the target surface. With this assumption, the equation is formulated as

$$c\rho \frac{\partial T}{\partial t} = I(z,t)\ \alpha + \frac{\partial}{\partial z}\left(k \frac{\partial T}{\partial z}\right),$$

where $I(z,t) = (1-R)I_o(t)e^{-\alpha z}$

with: c = heat capacity,

ρ = mass density,

α = absorption coefficient,

k = thermal conductivity,

R = reflectivity,

I = incident power density, and

z = distance from the surface along the incident light direction.

The solution to the equation is arrived at via numerical means to include phase transitions and changes of optical and thermal parameters with temperature and structure. The absorption coefficient is the factor responsible for the efficiency with which the material converts the photon energy into heat. The value of α is primarily dependent upon the sample structure and the wavelength of the incident electromagnetic radiation. For extrinsic crystalline silicon, the value of α is approximately 30 cm^{-1} as compared to 5×10^4 cm^{-1} for amorphous silicon. In addition, the results of experiments on the pulsed laser annealing of silicon have shown that infrared laser pulses are not as efficiently coupled to the solid as are pulses in the visible range of the spectrum (e.g., 694.3 or 530 nm) [Ref. 23].

Although the assumption of a beam with uniform intensity greatly simplifies the exercise of obtaining a solution to the modified heat diffusion equation, in actuality the pulsed laser beam is more accurately approximated by a Gaussian profile. In the thermal model of laser damage proposed by Bartoli et. al. [Ref. 24], a semi-infinite solid is irradiated by a Gaussian beam, $P(r) = P_o \exp(-r/a)$, where P_o is the peak laser power density. The energy density E_o required to damage the sample can be written

$$E_o = E_{\Delta T} \left[1 + \frac{k\tau\alpha\pi^{1/2}}{a \tan^{-1}(4k\tau/a^2)^{1/2}} \right] ,$$

where

$$E_{\Delta T} = \frac{\Delta T \rho c}{(1-R)\alpha} ,$$

k is the thermal diffusivity, ρ the density, c the specific heat, R the reflectivity, and α the absorption coefficient. ΔT is the increase in surface temperature at r = 0, which is required for damage due to melting. The quantity $E_{\Delta T}$ is the energy density required to raise the surface temperature by ΔT in the absence of thermal conduction. This theoretical formulation fits the experimental data fairly well, but the model suffers from one serious shortcoming. It neglects the

effects of electric field breakdown in the material and is therefore only valid for estimating damage thresholds when the irradiation times are sufficiently long so as to avoid these effects.

The two models presented here are typical of the many which have been proposed to describe the effects of laser radiation upon semiconductors. Despite varying levels of complexity and a diversity of physical assumptions in the development of these models, the most accurate methods of determining the thresholds for surface melting and damage are empirical.

Not all researchers are assured that the fundamental process involved in laser interaction with semiconductor targets is a simple thermal melting. A non-thermal theory proposed by Van Vechten [Ref. 25] postulates the existence of a dense electron-hole plasma excited by the pulsed laser radiation and which undergoes a boson condensation to a superfluid phase. At this time, the exact nature of the laser annealing process is still the subject of serious conjecture. The contradictory data which fuels the controversy over the thermal versus non-thermal modelling of laser annealing is obtained through varied experimental techniques. Among the more common procedures utilized to study the effects of laser irradiation of semiconductors are Rutherford back-scattering, Raman scattering, optical

microscopy, measurement of conductivity and other electrical properties, and perhaps most importantly and most often quoted, time resolved optical probing.

III. PREVIOUS WORK

A. SIGNIFICANCE OF TRR

The effects of laser radiation upon semiconductors are manifested in diverse ways. Thermal instabilities in detector material may render a device ineffective for time periods of several hundred milliseconds due to a single 200 μsec laser pulse [Ref. 26]. Variations in electrical properties due to pulsed laser irradiation have been well documented [e.g., Ref. 27]. Surface damage to semiconductor samples has been analyzed by a variety of methods. The value of optical and scanning electron microscopy in ascertaining the extent of surface damage can be readily seen. Yet, the most valuable data regarding the threshold values of laser energy density to produce surface damage and the nature of the damage mechanism are obtained via time-resolved reflectivity (TRR) measurements. Such time-resolved measurements provide the means to determine the time scale for energy transfer. They furnish direct, dynamic information regarding the melting and recrystallization process both during and nanoseconds after pulsed laser irradiation. This information can be employed to modify or verify the accuracy of theoretical models describing the laser-target interaction. Results of TRR

experiments are currently at the focus of the thermal versus non-thermal controversy over the nature of pulsed laser annealing of semiconductors.

B. MODEL FOR ANALYSIS OF TRR SIGNATURES

Figure 6 illustrates the model used by Lowndes and Wood [Ref. 28] to analyze TRR signatures. The model trace is typical of results obtained by other researchers [Ref. 23]. The TRR measurement is characterized by a reflectivity increase from the initial value R_s^o to the value for the liquid phase R_l^{max}. The rise time for the reflectivity increase is denoted by τ_r. The reflectivity remains at a value of R_l^{max} for the time indicated by τ_m Following the laser pulse, the material begins to cool and resolidify. The reflectivity then falls toward the value R_s^∞ with a 1/e fall time of τ_f. The surface is melted for the total time $\tau = \tau_m + \tau_f$. FWHM (full width at half maximum) is indicated by $\tau_{1/2}$. It is this model of TRR which was used to reduce the data obtained through this thesis experimentation.

C. OBSERVED RESULTS

The TRR traces and observed melting and damage thresholds show degrees of variance associated with the functional dependencies of these phenomena. A variety of laser wavelengths, spot sizes, energy densities, pulse widths, sample crystallographic orientations, and experimental

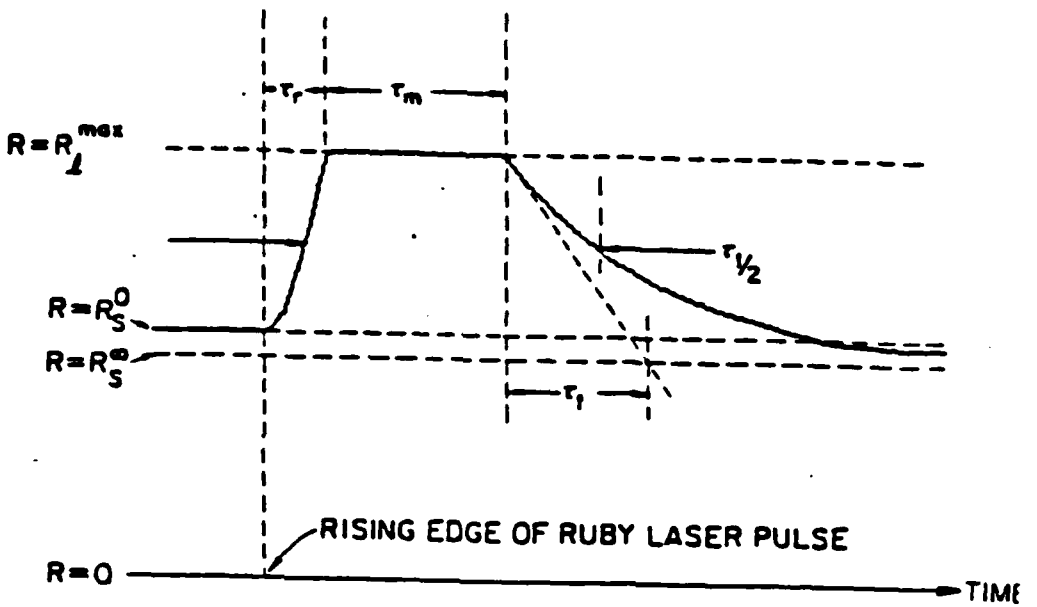

Figure 6. TRR Model Used in the Analysis of Pulsed Laser Irradiation of Semiconductors

geometries have been utilized in the investigation of TRR of semiconductors. An exposition of several researchers' work will now be presented. Having previously mentioned the dependence of optical heating upon the wavelength of the pulsed laser beam, previous work using visible and 1.06 μm pulses will both be reviewed.

In the work of Pospreszczyk et. al. [Ref. 29], single crystalline targets of Si(110) were irradiated at nearly normal incidence with pulses from a Q-switched ruby laser (20 ns. pulse length). The experiments were conducted in vacuo and the energy density of the ruby laser was varied by using absorption plates in the beam path. The diameter of the pulsed laser spot at the target surface was four mm. A cw He-Ne probe laser, with spot size diameter of 1 mm at the target, was reflected from the center of the ruby laser spot and sensed by a photomultiplier tube. Pulsed laser energy density readings were taken on each shot and were determined to be accurate within $\pm$ 10%. Typical traces of TRR from this research are shown in Figure 7. It was found that no change of reflectivity could be observed for energy densities below 0.5 J cm^{-2}. At higher energy densities, $\geq$ 0.8 J cm^{-2}, the increase in reflectivity occurred for every pulsed laser shot. This latter finding was taken to clearly demonstrate that Si is molten for energy densities above 0.8 J cm^{-2}.

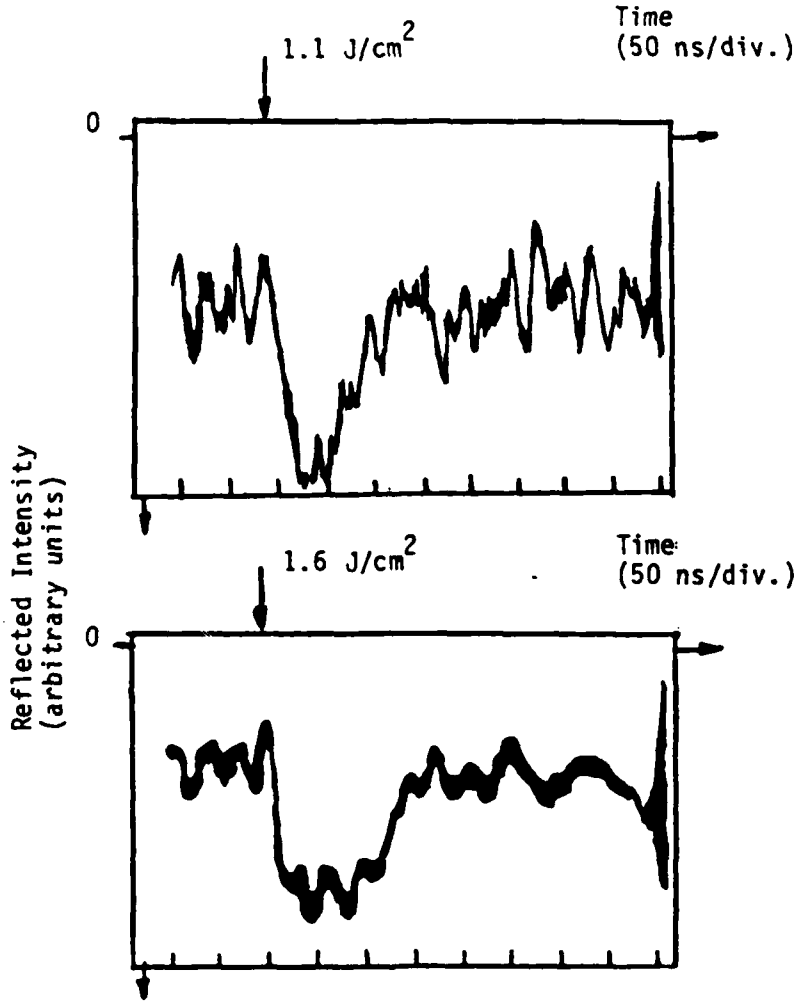

Figure 7. TRR of Si(110), After Pospieszczyk et. al.
(λ = 693 nm, annealing pulse)

Additional analysis of TRR in silicon irradiated with a pulsed ruby laser was undertaken by Galvin et. al. [Ref. 30]. Wafers of Si(111) doped with Au, were irradiated in air with a Q-switched ruby laser with pulse length 30 ns (FWHM). A quartz beam homogenizer was used to obtain uniform illumination of the target and neutral densitiy filters were employed to vary the incident laser energy. Again, a cw He-Ne laser was used to probe the surface reflectivity during irradiation with the ruby laser. The results of the experiments are depicted in Figure 8. It was concluded from interpretation of these results that the threshold energy density for melting of the extrinsic silicon was approximately 0.8 J cm^{-2}.

Experiments conducted by M. Takai et. al. [Ref. 31] investigated TRR in extrinsic silicon wafers, with crystallographic orientation (100). A Q-switched Nd:glass laser, operating at a wavelength of 1.06 μm and a pulse length of 20 ns, was used as the annealing beam. A quartz diffusing rod was used to achieve a homogeneous beam energy density profile. The reflectivity change of the sample surface was measured with a He-Ne probe laser incident upon the target and reflected onto a silicon p-i-n photodiode. The results of this experimentation are shown in Figure 9. Increases in reflectivity were observed for laser energy densities greater than 0.4 J cm^{-2}. For energy densities

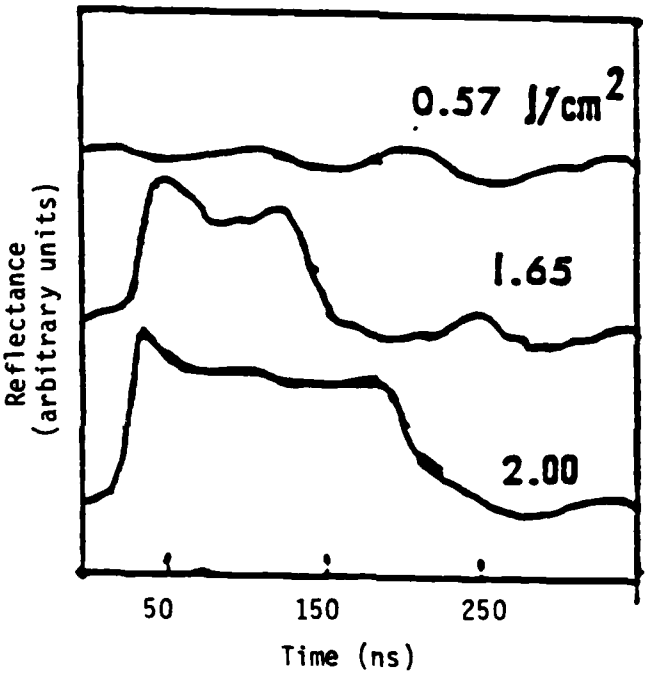

Figure 8. TRR of Si(111), After Galvin et. al.
(λ = 693 nm, annealing pulse)

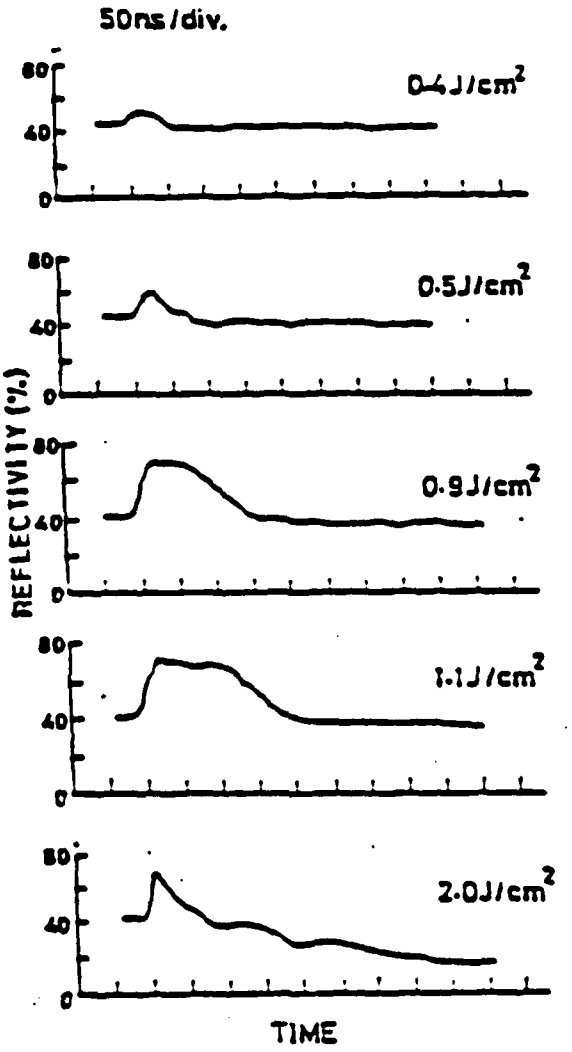

Figure 9. TRR of Si(100), After Takai et. al.
(λ = 1.06 μm annealing pulse)

greater than 2.0 J cm^{-2}, the reflectivity decreased after an initial rise due to surface damage caused by evaporation. Flat-topped reflectivity curves were obtained with laser energy densities of 0.9 and 1.1 J cm^{-2}.

Experiments at Oak Ridge National Laboratory by White, Narayan, and Young, were conducted in a fashion similar to Pospieszczyk et. al. The published findings of these experiments indicated that residual surface damage was observed for boron, arsenic, and phosphorous implanted silicon after irradiation with laser energy densities of approximately 1.1 J cm^{-2} [Ref. 33].

This review has demonstrated a reasonable degree of agreement among researchers regarding the observed threshold for laser-induced surface damage in extrinsic silicon targets. The nominal value for such damage would seem to be between 0.8 and 1.1 J cm^{-2} for annealing laser pulse widths of 20-30 ns.

IV. EXPERIMENTAL DESIGN AND METHOD

A. EXPLANATION OF APPARATUS

Comparison of time-resolved reflectivity signatures of P-doped silicon versus incident Nd:glass laser energy was performed using the experimental setup shown in Figure 10. A sense of the nanosecond time regime must be had in order to appreciate the complexity of this construction. This ultra-short time scale and the need for electromagnetic (EM) noise elimination, as will be discussed later in this section, became the driving and dominant factors deciding the final layout of equipment as well as forcing the experimenters to manufacture a suitable detector. Numerous other pieces of electronic gear were tried unsuccessfully before arriving at the final selection and setup of equipment. In addition to that shown in Figure 10, a Bausch-Lomb optical microscope and a Perkin-Elmer spectrophotometer were employed in the course of experiments for this thesis. A more detailed description of the apparatus follows.

1. Laser System

In order to investigate the nanosecond regime of time-resolved reflectivity of silicon, a high power, short pulse-width laser was needed. The Korad K-1500 neodymium-glass laser with amplifier was found to be a suitable system

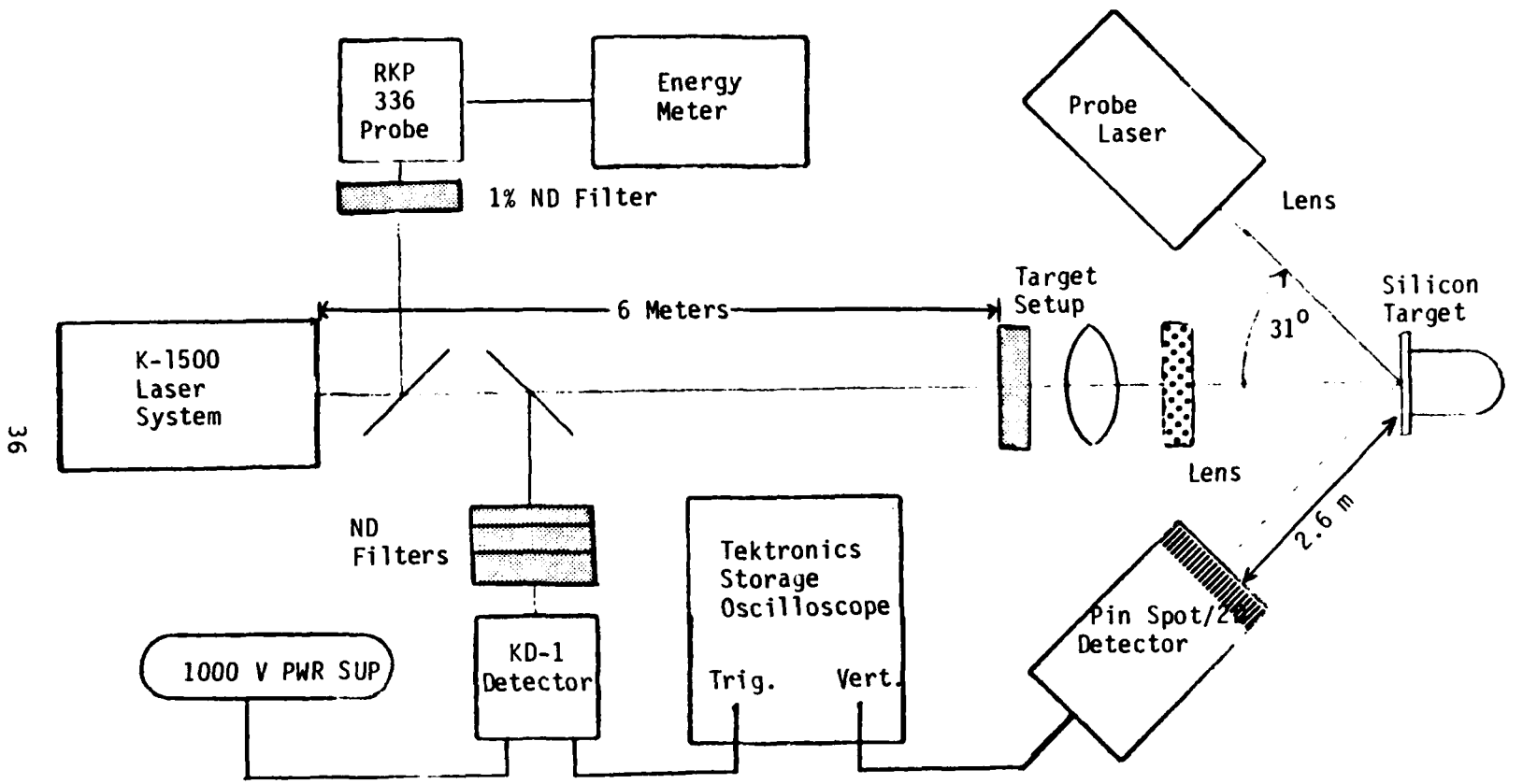

Figure 10. Experimental Design

boasting 600 MW of output power and a 20 ns full width at half maximum (FWHM) pulse shape. The wavelength of Nd:glass radiation is 1.06 micrometers. The output energy of the Korad K-1500 system can be changed by varying the applied voltage to the oscillator and amplifier flashlamps. A typical energy reading with the oscillator flashlamp voltage set at 5kV and the amplifier flashlamp voltage set at 7.5kV was found to be approximately 3.33 Joules. Over an average of 15 shots, the laser output energy varied $\pm$ 9%. The energy measuring technique will be discussed later in the procedures section. During the experiment, it was found to be more convenient to employ neutral density (ND) filters in the beam path, thus changing energy levels on the target. This method proved to give more reliable and predictable energy readings rather than changing the voltage applied to the flashlamps.

The K-1500 series employs a Brewster polarizing stack and a Pockels cell for cavity spoiling (Q-switching) of the K1 oscillator. The K2 amplifier increases the oscillator energy about five-fold during a single pass. Expansion optics are required between the K1 (oscillator) and the K2 (amplifier) to expand and recollimate the beam for the larger diameter K2 glass rod. A 0.6 mW helium neon laser is permanently mounted on the optical bench. This is continually used to check the laser system alignment and

that of all optics and target material further down the beam path. A maximum pulse repetition rate of one per minute can be safely used on this system. A more detailed description of the installation and operation of the K-1500 series laser is given by Davis [Ref. 34]. Figure 11 displays a schematic representation of the laser system.

2. Energy Meter

As well as investigating time-resolved reflectivity, the energy density threshold for surface damage was experimentally found for p-doped silicon. The Laser Precision Corporation RK3230 energy meter with RKP 336 probe was used to measure laser output energy and determine energy density on the target. The mechanics of determining target energy density will be discussed in the procedures section. As shown in Figure 10, the beamsplitter, an optical glass slide, sent four percent of the laser energy to the RKP probe. However, eight percent of the total laser energy was lost due to a four percent reflection at each air-glass interface. Overall, the transmission of one optical glass slide at 1.06 μm is ninety-two percent. This percentage was verified at the appropriate wavelength using an IR spectrophotometer. A one percent transmission filter was used to protect the RKP probe from damage due to excessive laser fluence.

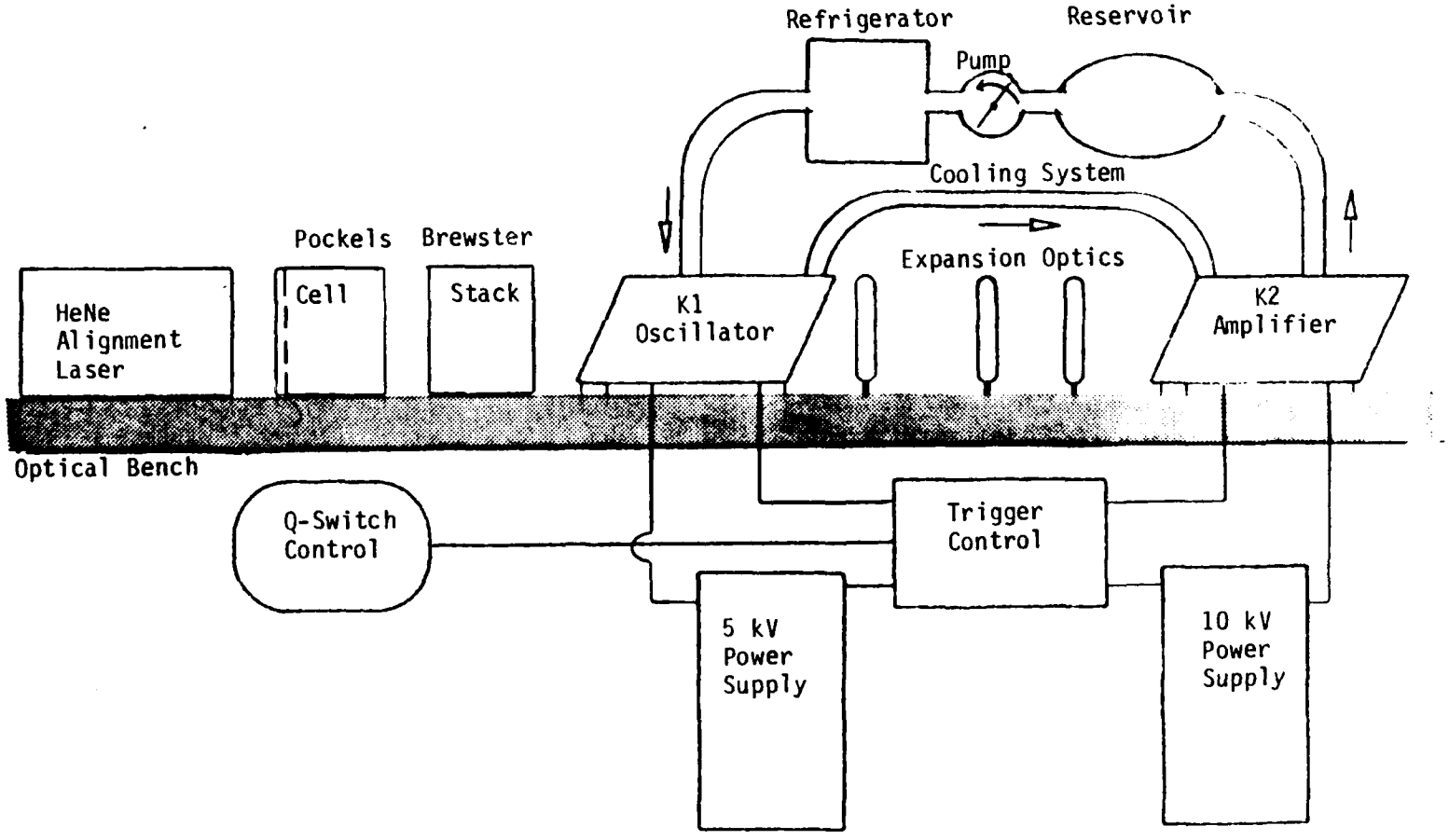

Figure 11. The K-1500 Laser System

The IR active device employed by this system is a pyroelectric detector. When used with the accompanying signal processing and display electronics, this sensor is intended to measure the total energy content of radiation pulses with durations ranging from one nanosecond to one millisecond. The maximum energy that the probe may safely sustain before damage occurs is ten joules.

3. Oscilloscope

In order to investigate the dynamic behavior of pulsed laser annealing processes, a storage oscilloscope with nanosecond resolution and high persistance was needed. The Tektronix 7834 storage oscilloscope, with 7A24 vertical amplifier and 7B80 horizontal time base installed, was used. This combination offered a bandwidth of 300 MHz, but more importantly, a rise time of 1.2 nanoseconds. Incorporated in the vertical system of the Tektronix 7834 is a delay line which permits viewing of the leading edge of a trigger signal. This delay line insures the oscilloscope is triggered before any information is sent to the vertical display. The 7A24 vertical amplifier also offered a two channel summing capability which became extremely important for electromagnetic noise elimination, as will be discussed later. One drawback of the 7A24 is a maximum input voltage of seven volts peak. Some unsuccessful attempts early in the experiment used detectors which would easily exceed the

seven volt limit. However, the detector finally settled upon, presented no problem as output voltage never exceeded 100 mV. The 7834 storage oscilloscope proved to be a highly flexible measurement system with its high vertical bandwidth and fast storage writing speed.

4. Trigger Source

A reliable and rapid response trigger signal for the Tektronix oscilloscope was needed for the time sensitive measurements of the nanosecond regime. Initially, the output trigger provided by the shutter control unit, which controls the Pockels cell, was used. However, this trigger signal later proved very inconsistent and unreliable. The Pockels cell is charged 450 μs before the laser fires. Therefore, the trigger from the shutter control unit, which controls charging of the Pockels cell, had to be delayed 450 μs $\pm$ 40 ns before starting the horizontal trace of the oscilloscope. Since all pertinent information on time resolved reflectivity occurs within the first 150 ns of laser energy interaction with target material, the oscilloscope trigger must occur a few nanoseconds prior to laser beam coincidence with the target. The problem of delaying the shutter control trigger (450 μs $\pm$ 40 ns) proved insurmountable. Several attempts were made using two different delaying systems. First, the BNC Digital Delay Generator, model 7010, was tried in several different

operating modes without success. Even though the BNC delay generator worked properly on the test bench, it was inconsistent when used in the experiment, many times providing no trigger signal at all. A second attempt at delaying the shutter control trigger was made using the Tektronix 7B85 Delaying Time Base plug-in module on the oscilloscope. This unit, when used with its companion, the 7B80 Time Base, is capable of time delays in the range required; however, the specified accuracy, $\pm$ .005 times the set delay, produced a retardation of 450 µs $\pm$ 2.3 µs which proved much too large for this experiment.

As the investigation for a delay system continued, it was discovered that the shutter control trigger was not consistently 450 µs prior to laser firing. This led to the abandonment of the shutter control unit as a trigger source.

The final solution of the trigger problem rested with a second beam splitter, a glass slide, and a fast detector. The Korad KD-1 Photodiode was used in conjunction with the Precision DC High Voltage Source, Model 1565, which provided the KD-1 bias voltage of 1000 volts. This system incorporates a rapid response planar diode tube and can give simultaneous measurements of both the power and the energy output of a laser beam. Since the KD-1 calibration had expired, it was decided that its output would be used as a trigger source rather than as an energy or power measuring

source. The recommended setup for this laser monitoring device includes a MgO diffuser block which acts as a point source whose intensity attenuates as $1/R^2$. When placed in the beam path after the glass slide beam splitter, this diffuse surface reflects approximately 97% of the incident radiation, obeying Lambert's Law for angular dependence of the reflection. The photodiode is then placed an appropriate distance from the MgO block to attain the required output signal level. This configuration, which was found to be quite clumsy, was modified as shown in Figure 10, and the MgO block was discarded. Three neutral density filters, giving a combined transmission of 0.1%, were used in the beam path prior to the KD-1 detector. This produced a suitable trigger signal of approximately fifteen volts peak from the power output connector on the rear panel of the KD-1 assembly. In order to preserve the detector's rapid response time, the energy output connector, also on the rear panel, was terminated by a fifty ohm load in accordance with the manufacturer's instructions. In the configuration described above, the KD-1 sensor became an extremely reliable and fast response trigger source with a rise time of only a few nanoseconds. This system consistently delivered trigger signals approximately twenty-five nanoseconds prior to the detection of laser energy-target coincidence.

5. Probe Lasers

A secondary intention of this thesis was to see how time-resolved reflectivity varied with changes in probe laser wavelength. Figure 12 shows a plot of reflectivity versus wavelength of the polished silicon wafers used in this experiment. To test this subordinate objective, two probe lasers were chosen in the visible range: Argon-Ion with a wavelength of 488 nm, and Helium Neon with a wavelength of 632.8 nm. Since Figure 12 shows a similar reflectivity of approximately forty to forty-five percent at these two wavelengths, time-resolved reflectivity should not vary significantly with these two probe lasers. Data was taken, analyzed, and compared with the HeNe and ArIon lasers with results in the following section.

The HeNe laser used was manufactured by Hughes Corporation and gave an output power of four milliwatts. The Ar-Ion laser was a product of Spectra-Physics with ten milliwatts of output power. Other, lower power, lasers (< 1 mW), were available but proved less profitable as the sensing detector needed relatively high power to produce a good DC output signal from the probe lasers.

6. Target Setup

Considerable care was taken in the target setup details to guarantee the consistency of observed results. To properly measure time-resolved reflectivity, the

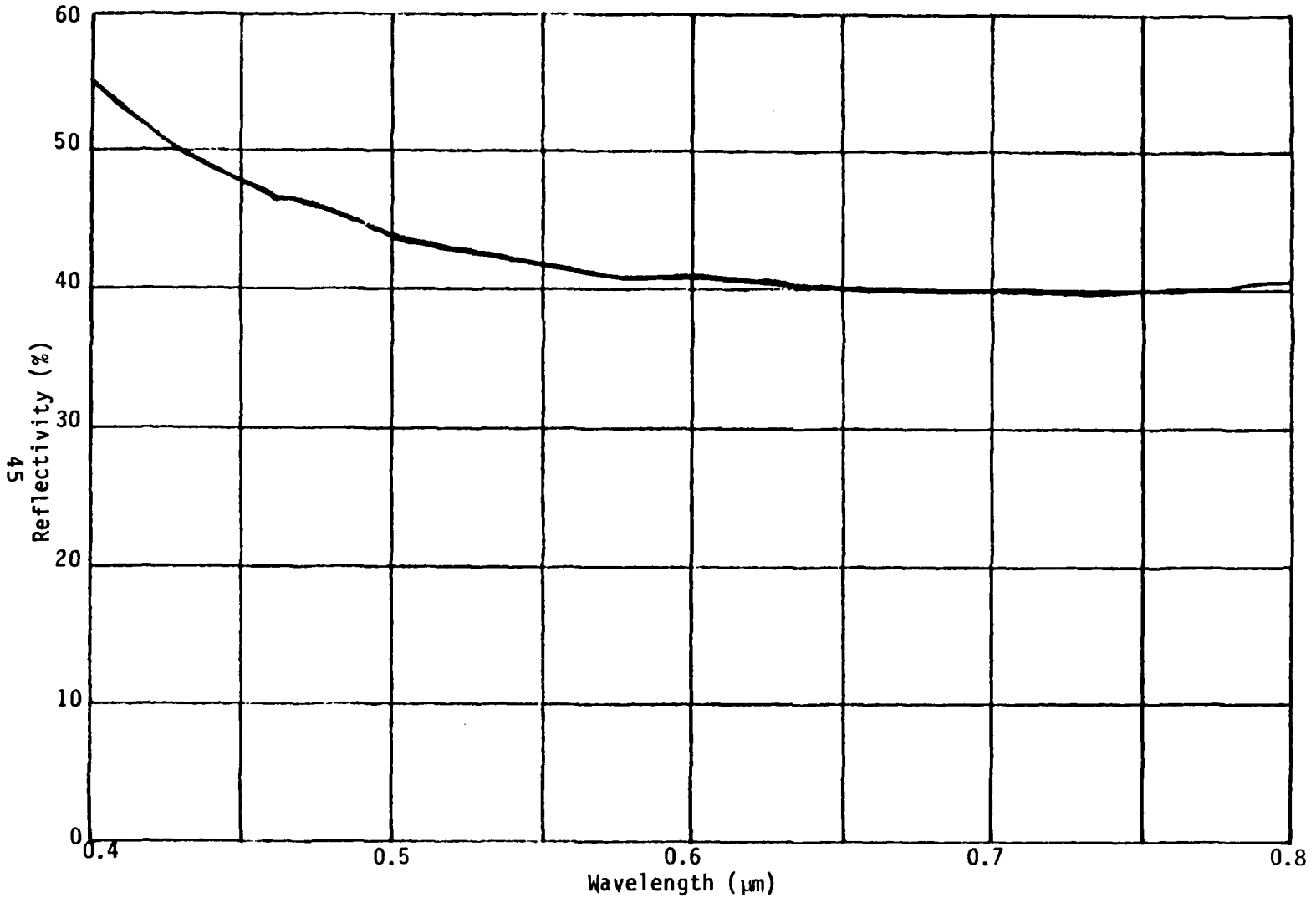

Figure 12. Reflectivity Versus Wavelength for Polished Silicon Sample (Obtained from Spectrophotometer)

experimenter must insure that the annealing laser beam possesses the following three characteristics:

1. variable power levels,
2. measurable and reproducable spot size,
3. spatially homogenous levels of energy density.

Figures 13 and 14 show the arrangement used to accomplish these requirements.

As previously discussed, the Nd:glass laser energy was modified using neutral density (ND) filters of varying transmittance. This method proved to be simple and quite accurate as each ND filter's transmittance was verified at 1.06 micrometers, the annealing laser's wavelength, using the Perkin-Elmer spectrophotometer. Thus, the first characteristic of the annealing beam was accomplished. Unfortunately, the second and third requirements were not as easily fulfilled. Since the second characteristic became a function of the arrangement used for spatial homogeneity, it will be briefly discussed last.

Figure 15 is a photograph of the laser beam profile (laser spot) produced by the Korad K-1500 system. Unfortunately, there is no practical method of measuring the exact energy density in any part of the beam, since numerous "hot spots" exist in the profile. Other researchers in time-resolved optical studies have encountered this problem and offered various solutions. In fact, a few papers have been

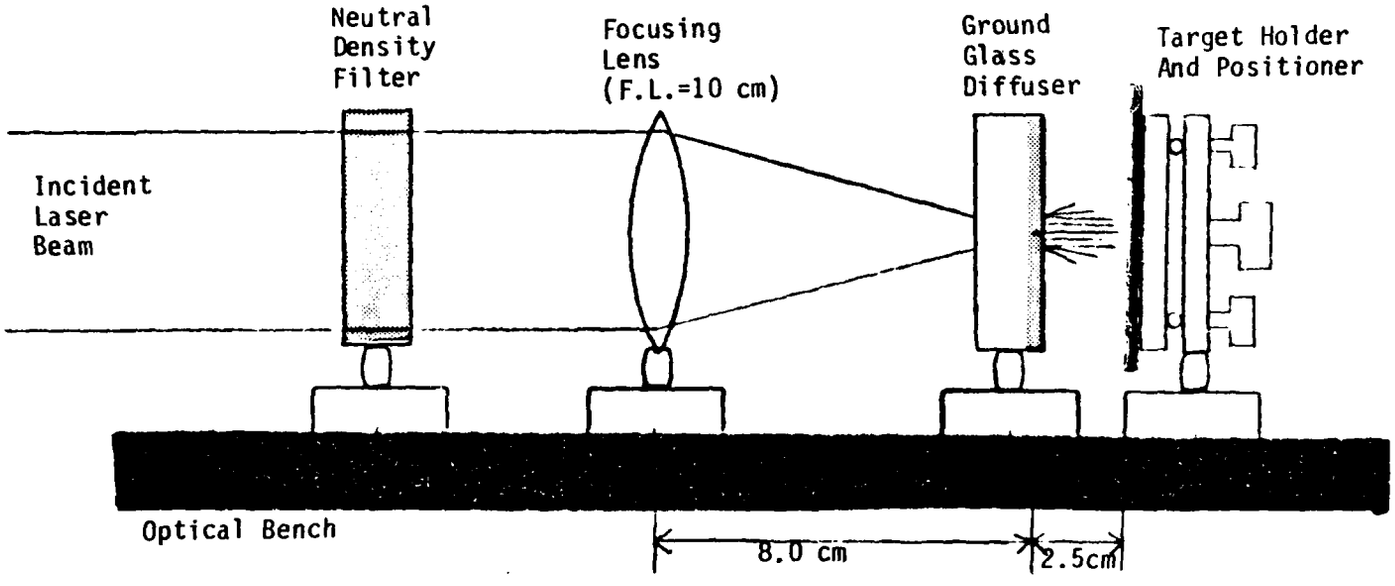

Figure 13. Schematic Diagram of Target Setup

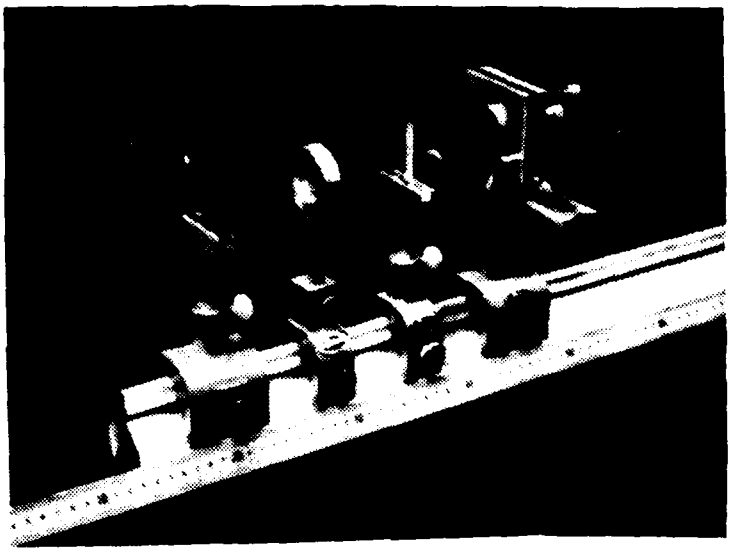

Figure 14. Photograph of the Target Setup

Figure 15. Laser Spot Produced from the Korad K-1500 Laser System

published that deal strictly with homogenizing laser beam profiles [Ref. 35]. Solutions of this problem vary, but a few are worth mentioning. A quartz diffuser, sometimes called a diffuse quartz "light-pipe", has previously been used with good success. This pipe-shaped quartz crystal scatters the incoming laser beam and produces an output profile that is uniform in cross-sectional energy density. Within a few millimeters of the output end of the crystal, one can say the energy density is homogeneous across the center of the beam profile. Another, simpler method of accomplishing this task uses a mask near the target to block all of the incident radiation except a small portion that is judged to be consistently homogeneous. The laser energy that passes through this small aperture is then measured so an energy density may be established. However, this procedure reduces considerably the maximum output power available. A third method, which was chosen for this experiment, is very similar to the quartz diffuser but uses ground-glass as the diffuse medium. The range of angles through which light is scattered is a function of the diffuser structure. Ground glass screens scatter most incident light into a narrow cone about the beam axis [Ref. 35].

By using a lens to focus the incident laser beam to a small spot ($\approx$ 2 mm) on a ground glass surface, a Gaussian

shaped profile of energy density is observed a few centimeters aft of the ground-glass. The diameter of this modified beam, as shown in Figure 16, was approximately one centimeter and it was determined to have a uniform energy density over a two millimeter diameter circle centered on the laser spot. For this reason, the probe laser beams were focused down to a small spot size (approximately one millimeter in diameter for the HeNe laser and two millimeters for the Ar-Ion laser) and centered on the annealing beam spot. Figure 17 shows a graph of normalized intensity versus distance across the laser beam profile of the modified annealing laser and the probe laser. Near the center of the Nd:glass laser's gaussian profile, the beam intensity is approximately uniform. The focusing distance and ground-glass to target distance are critical to maintain a good profile and are shown in Figure 13. This optical arrangement also produced a beam spot size that was easily reproducible. The beauty of this setup is its ability to accomplish the desired annealing beam characteristics with relative simplicity.

Figure 13 also shows the target and target holder. Polished silicon wafers were chosen for this experiment as silicon is a basis material for many commercial and military electro-optic sensing systems. These wafers are device-grade polished silicon crystals doped with boron. The

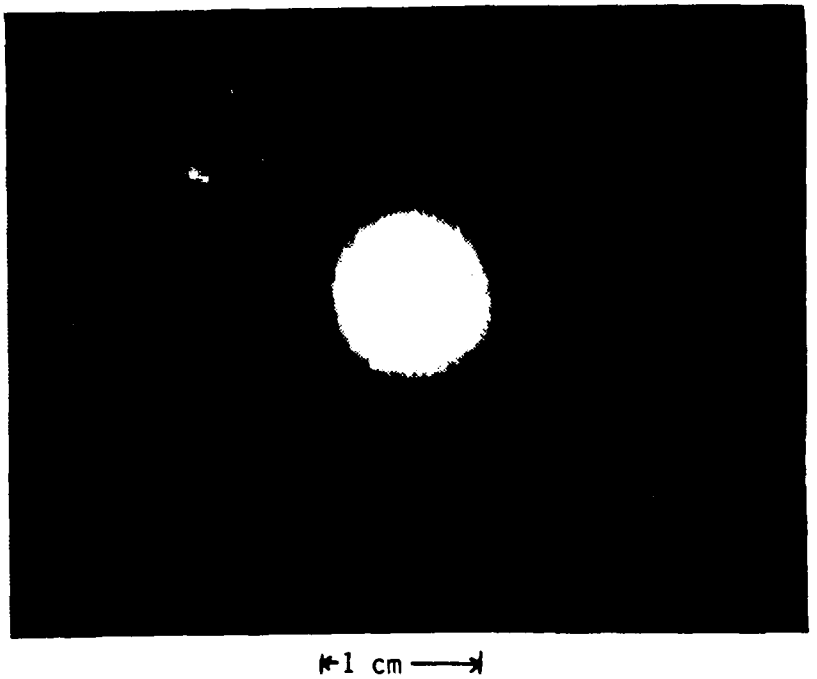

Figure 16. Laser Spot Produced After Beam Modification

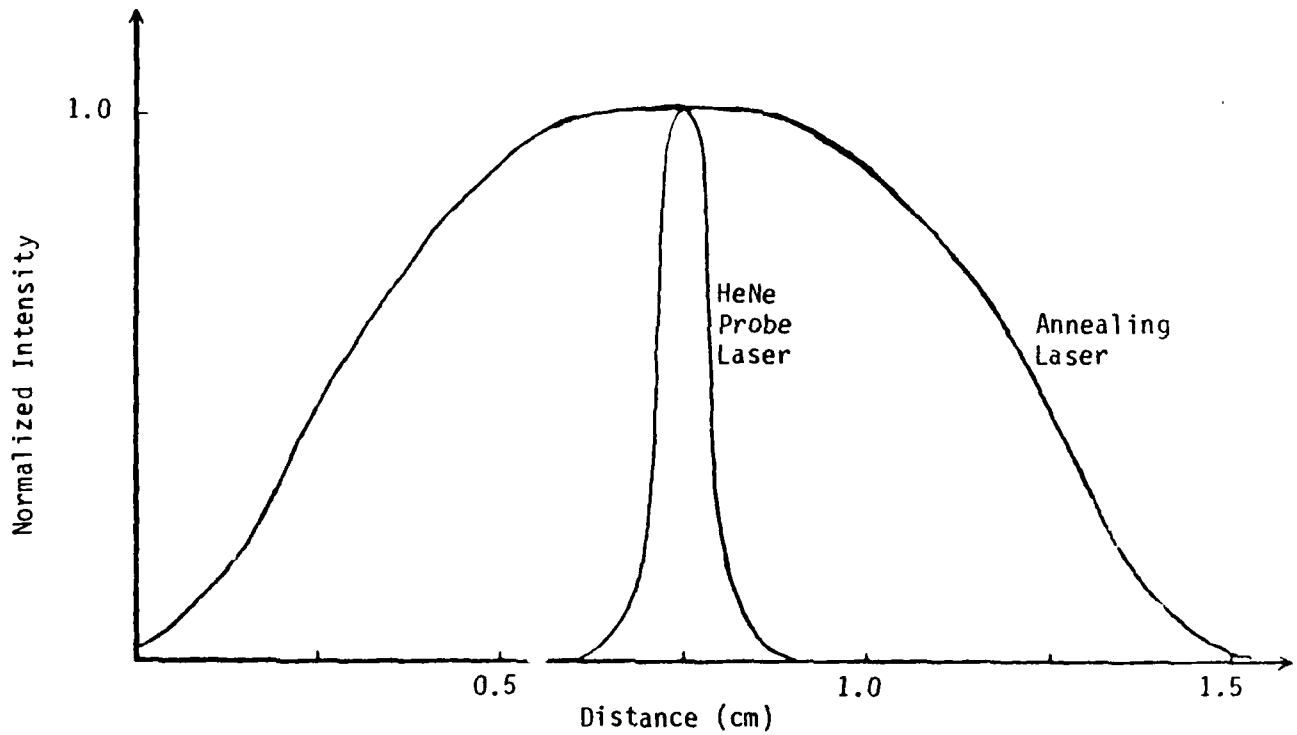

Figure 17. Approximate Beam Cross Section at Silicon Target

crystal orientation is 1-0-0. The target holder was manufactured locally and the features of its construction saved enormous amounts of time during experimentation. After each shot of the annealing laser, the silicon target had to be moved to ensure each test used a virgin site. After moving the sample, the probe laser beam had to be realigned so it reflected off the sample, directly into the sensing detector. All of these actions could be accomplished by adjusting the target holder-positioner. Once the silicon wafer was attached to the holder, it could be rotated about the annealing beam axis and also moved horizontally across the beam axis. In this way, any target site could be placed in the annealing beam path. In addition, two micrometer adjustments on the holder were available to position the reflected probe laser beam onto the sensing detector several meters away. If the annealing beam path is called the X-axis of a three dimensional cartesian coordinate system, the target holder allowed rotation of the sample about the Y-axis with one micrometer and rotation about the Z-axis with the other. This holder-positioner saved considerable time and effort during each target and laser alignment procedure conducted, prior to every test shot. This procedure will be discussed in detail later.

7. Detector

Measurements of TRR require a low noise detector with rapid response time and sufficient DC or quiescent output from probe laser irradiation. The sensor that best fit both of these requirements was locally designed [Ref. 36] and constructed using a United Detector Technology (UDT) PIN SPOT/2D detector element. Since it has been suggested that continuing research in this area may be pursued and other postgraduate students may require this detector, a list of the PIN SPOT/2D's specifications is given in Table I, and Figure 18 shows its normalized spectral response curve. Figure 19 is the schematic diagram of the detector with its impedance matching circuit. To obtain a sufficient quiescent output signal, large enough to overcome the noise signal, while the continuous wave probe laser illuminated the sensor, a large resistance is needed from the reversed bias detector element to ground. On the contrary, a small resistance is needed to obtain a small RC time constant, thus ensuring a rapid response time. Two thousand ohms proved, by trial and error, to be a good compromise resistance value. If the output voltage across the resistor was fed into the vertical amplifier of the storage oscilloscope, which has a fifty ohm input resistance, an impedance mismatch occurred, loading the sensing element and reducing the quiescent output voltage. For this reason, an

TABLE I

UDT PIN SPOT/2D SPECIFICATIONS

Active Surface Area	6.45 mm^2
Responsivity	0.3 A/W @ 632.8 nm
Dark Current	.009 µA @ 25 V
Capacitance	50 pf @ 0 V 11 pf @ 10 V 7 pf @ 25 V
N.E.P.	7×10^{-14} W/ Hz

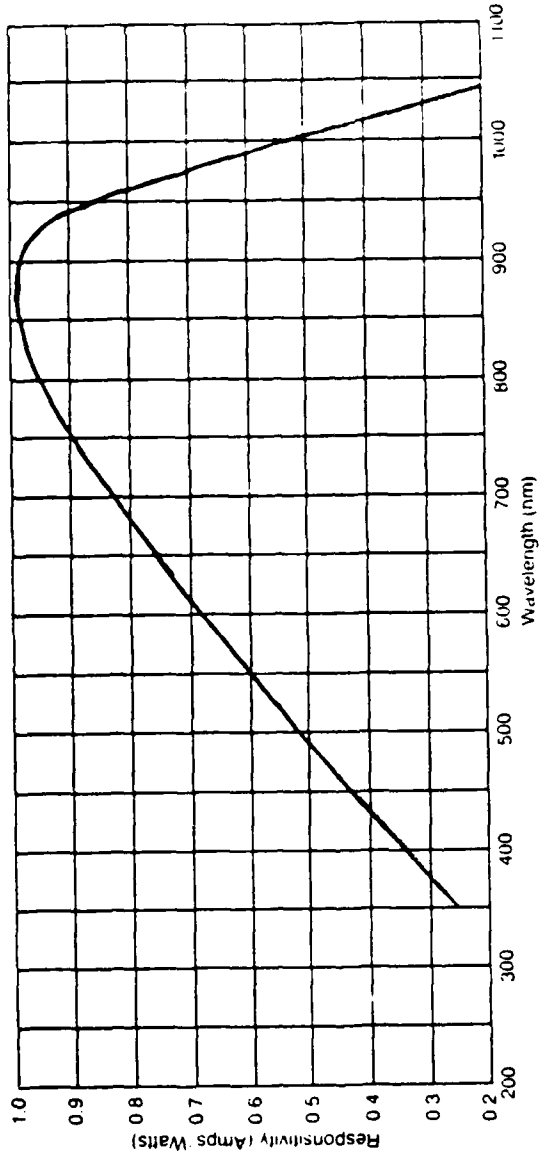

Figure 18. Normalized Spectral Response for the PIN SPOT/2D Detector

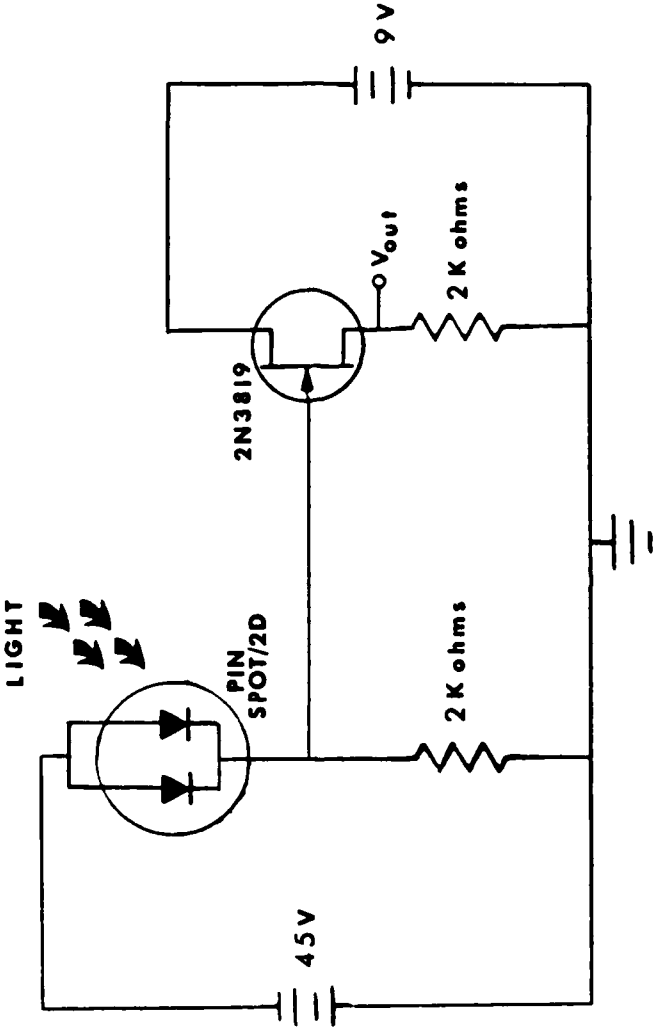

Figure 19. Detector with Impedance Matching Circuit

impedance matching circuit is required as shown in Figure 19. The detecting element is connected to the gate of a field effect transistor (FET), an infinite resistance. The only load seen by this element is its own 2KΩ resistance to ground. The oscilloscope, looking back through the drain of the FET, sees a Thevenin equivalent resistance of approximately fifty ohms, thus ensuring a fast RC time constant for the oscilloscope input. The detector impedance and the oscilloscope impedance are matched by this circuit. For future reference, a block diagram and an actual photograph of the detector are shown in Figures 20 and 21. The dummy BNC connector was used for electromagnetic noise elimination.

The method used to check the detector rise and fall (recovery) times was to compare an oscilloscope trace of the Nd:glass laser's output pulse using the locally constructed detector and another detector with known rise and fall times. The Lasermetrics Model 3117 photodetector was chosen for this comparison as its rise and fall times are less than one nanosecond. As Figures 22 and 23 demonstrate, the oscilloscope trace produced by the PIN SPOT/2D detector is nearly identical to that produced by the Lasermetrics. From this evidence and the manufacturer's specifications, the experimenters calculated the rise and fall times of the locally constructed detector to be approximately ten

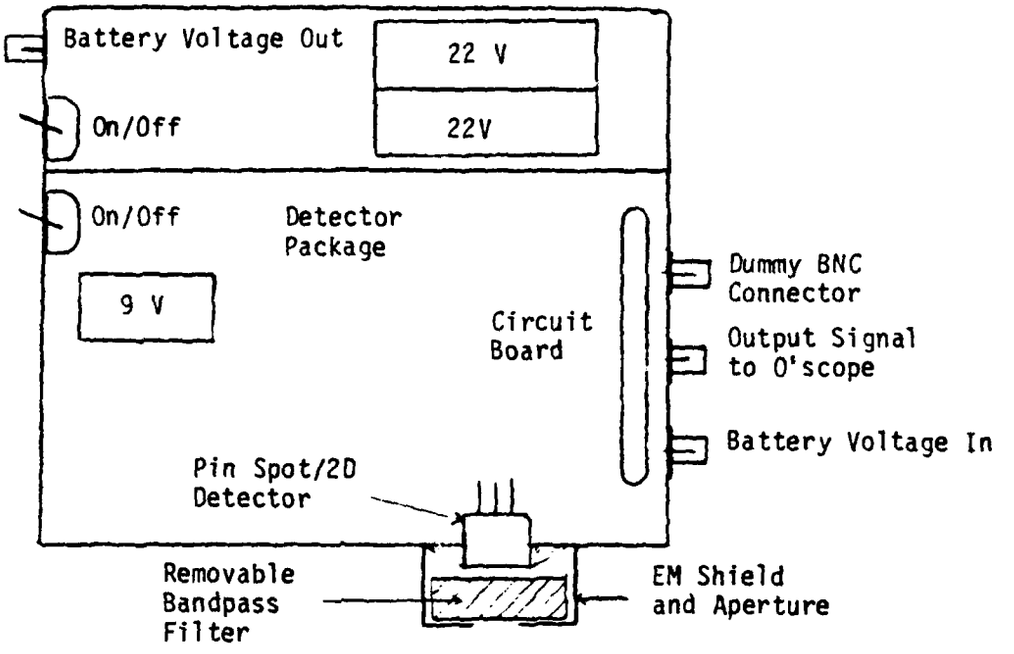

Figure 20. Block Diagram of Locally Manufactured Detector

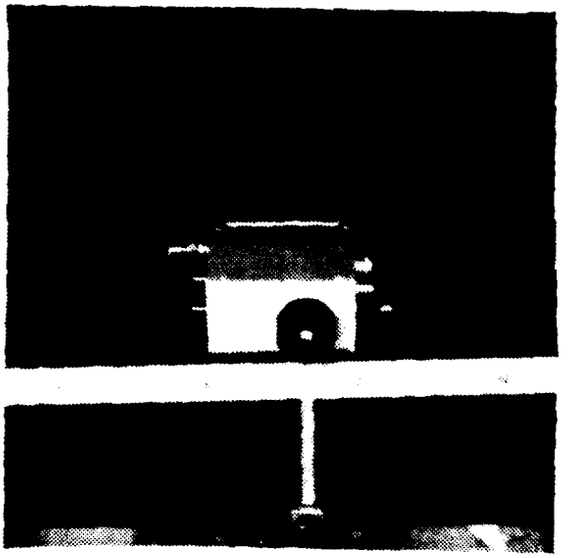

Figure 21. Photograph of Locally Manufactured Detector

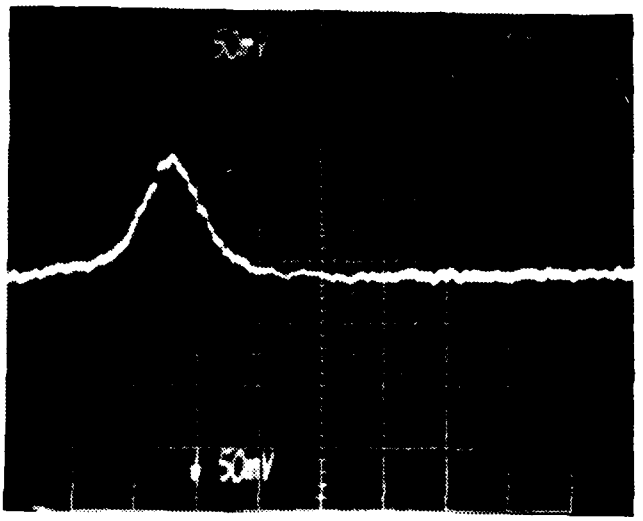

Figure 22. Neodymium Glass Laser Pulse as Seen by the PIN SPOT/2D Detector

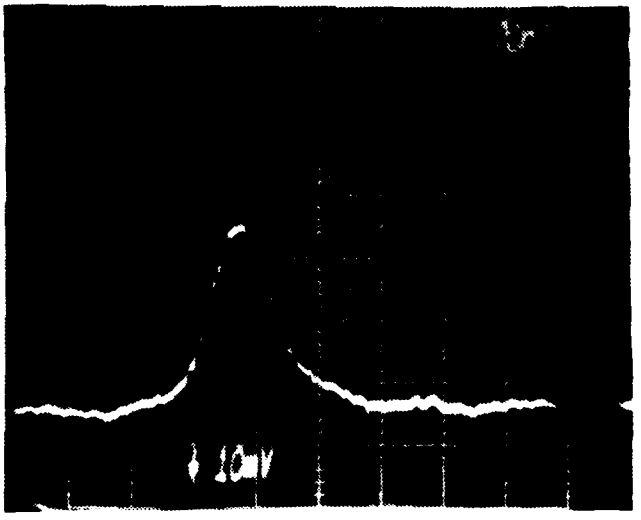

Figure 23. Neodymium Glass Laser Pulse as Seen by the Lasermetrics Detector

nanoseconds. Figure 24 is a graph of relative capacitance versus reverse bias voltage for the PIN SPOT/2D detector. Using a capacitance value of 5.1 pf, which corresponds to a reverse bias of 45 volts, and a resistance value of 2K ohms, the rise time was calculated to be 10.1 nanoseconds. These rapid response times are required for time resolved reflectivity measurements.

8. Equipment for Reflection Measurements

Figure 25 is a schematic diagram of the apparatus used to record the spatial intensity distribution of the HeNe probe laser beam reflected off a silicon sample before and after target damage. The photo-multiplier tube was mounted on a micrometer slide which, rotated by hand, moved the photo-multiplier across the observation plane. A narrow vertical slit (0.2 mm wide) aperture was used on the photo-multiplier to obtain an average value of the light field. The information from the photo-multiplier was amplified and sent to the X-Y recorder where a spatial plot of the reflected laser beam was transcribed. This system was used to determine the manner in which specular and diffuse components of reflectivity change under the influence of laser irradiation.

B. PROCEDURES

1. System Alignment

To ensure that accurate and reproducible data were obtained for every laser shot, an elementary alignment

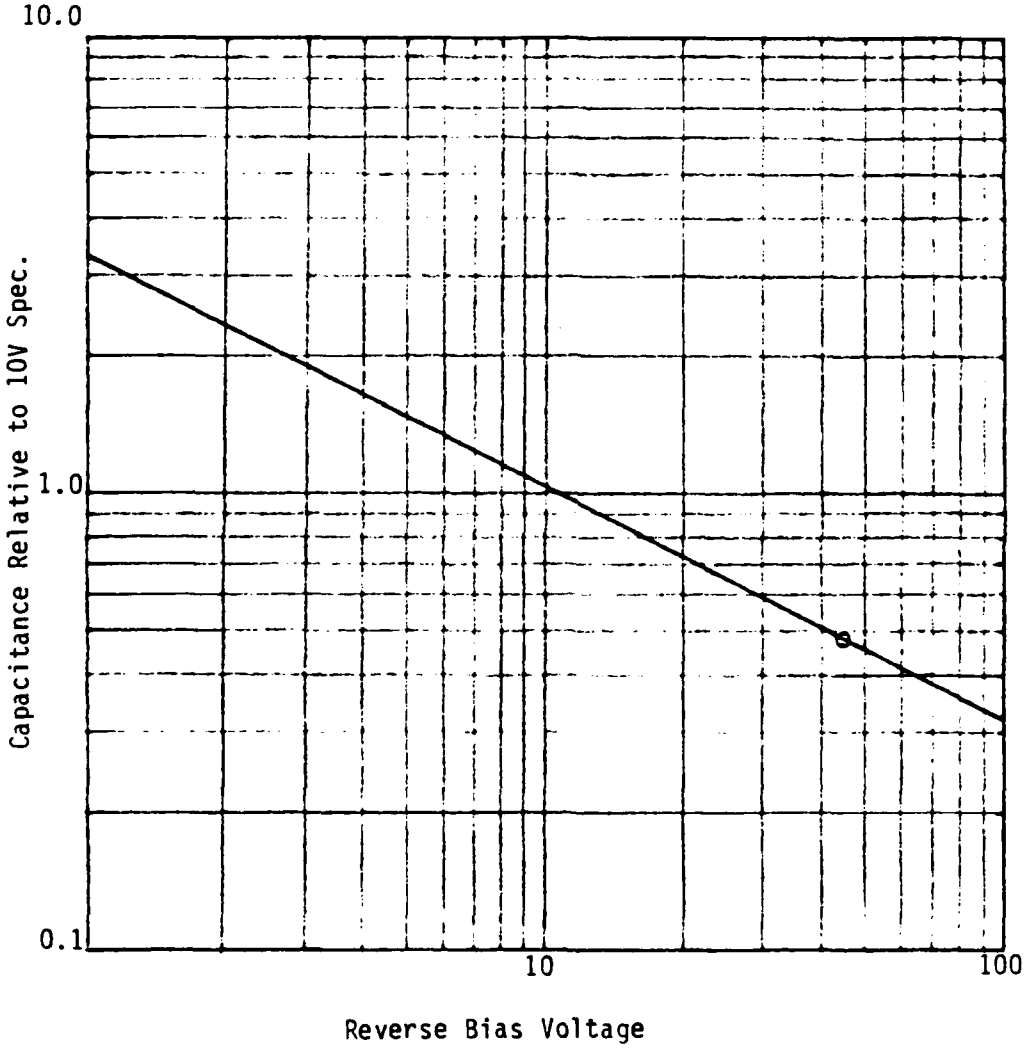

Figure 24. Relative Capacitance Versus Reverse Bias Voltage

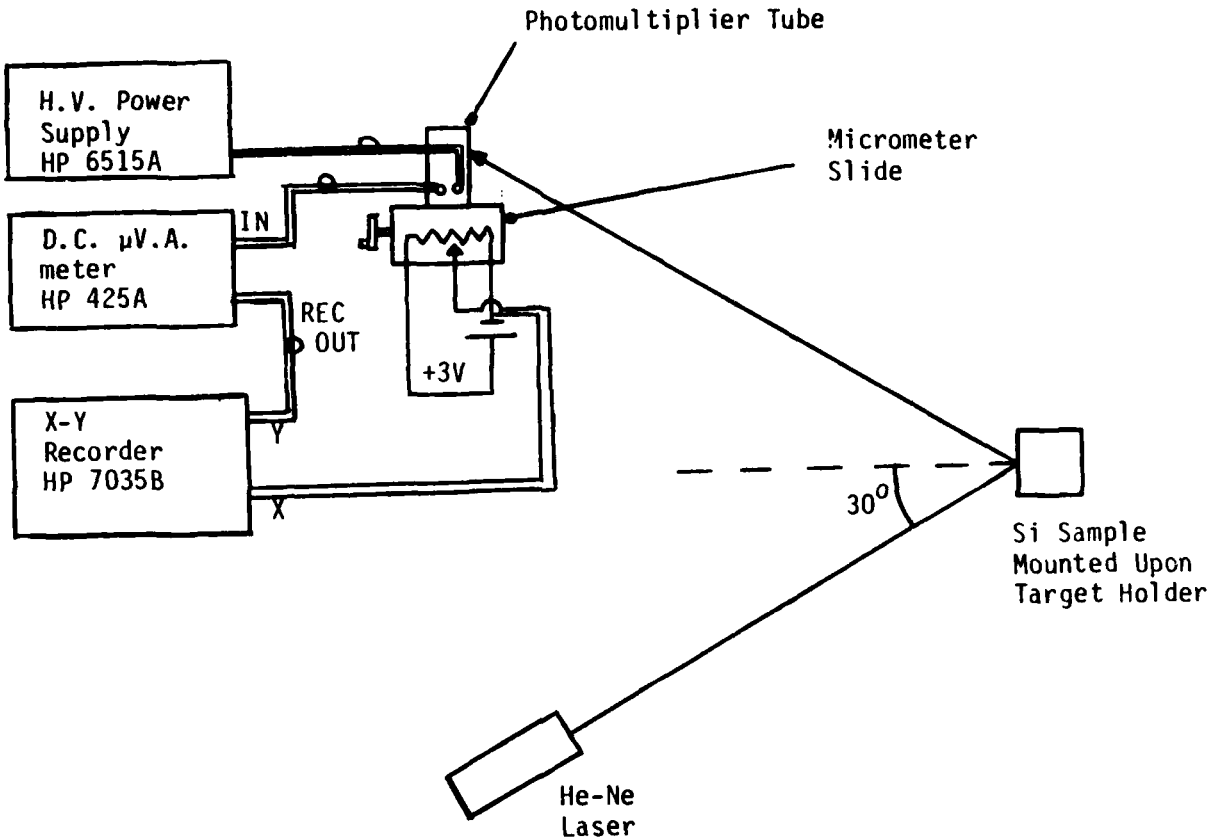

Figure 25. Schematic Diagram of Apparatus Used to Examine the Components of Specular and Diffuse Reflection

procedure was followed. After the Nd:glass laser was fired and data recorded, the target sample was repositioned using the holder-positioner previously discussed. This was done to provide a virgin site on the target material for each test run. Next, the probe laser spot was matched with the spot from the HeNe alignment laser on the K-1500 system. This step insures that the sample is uniformly irradiated at the probe laser spot where reflectivity charges are measured. Then the two micrometer adjustments on the holder-positioner were used to align the reflected laser beam directly on the sensing detector, maximizing its output voltage. A typical DC (quiescent) output voltage from the detector was forty millivolts using a HeNe probe laser. The final step was to verify again probe laser and alignment laser spot coincidence.

2. Energy Measurements

In the path of the annealing beam are two glass slide beamsplitters, one ND filter, one lens and a slide of ground glass prior to the silicon target. Since the energy meter measures laser output energy before the beam is modified, the actual energy on the target cannot be easily calculated, particularly since a diffuse medium lies in the beam path. To overcome the mathematical difficulty of trying to calculate the energy deposited on the silicon sample, the following method was used.

First, the average output energy of the K-1500 laser system was measured after a sufficient "warm-up" period. This was accomplished by averaging a series of fifteen laser firings timed two minutes apart. Consistent time intervals between shots proved to give more consistent output energy levels from the Korad laser system.

Next, the energy meter probe was moved to the exact position that the target occupies, keeping the identical spacing as was maintained between the ground glass and the target. The glass slide beamsplitter used in conjunction with the energy meter was left in the annealing beam's path. With the energy meter in this new position, another series of fifteen equally spaced laser shots was taken. From the mean values of the two series of energy readings, a percentage of energy transmitted to the target was calculated. This value was 59.5%. Therefore, the actual value of energy on the target is 59.5% of the energy measured at the output of the K-1500 laser system. This percentage applies only when the ND filter is absent. When a ND filter is present, the 59.5% value must be multiplied by the transmittance of the filter.

For laser pulses whose energy is within one standard deviation of the mean laser output energy reading, the approximate error in energy measurement is 10%. This figure was determined through consideration of the value of the

standard deviation of laser pulse energy, the inherent detector measurement error, and the error in the listed values of percentage transmittance for the ND filters. As was previously mentioned, numerical values for the percentage transmittance of the ND filters at 1.06 μm were obtained experimentally through use of the Perkin-Elmer near infrared grating spectrophotometer.

The most important parameter of these measurements is the energy density at the target surface. This was easily computed by keeping specified distance between the focusing lens, ground glass and target, thus maintaining a constant spot size of $\pi/4$ cm^2 on the silicon sample. For these energy density computations, a uniform beam profile was assumed.

3. Noise Reduction

It has been suggested that continuing research in TRR and electro-optic device damage due to laser irradiation be conducted at the Naval Postgraduate School. For this reason, a detailed analysis of noise elimination procedures will be discussed, in the hope that future students may gain from the lessons learned during this experimentation. The K-1500 laser system produced two types of noise that had to be eliminated or considerably reduced before any useful information could be obtained from the experimental apparatus previously described. These two classifications

of noise were high frequency electromagnetic and optical. Each will be discussed separately.

Two self-contained, cabinet-style power supplies accompany the K-1500 laser system; one capable of charging up to 5 kV for the laser oscillator, and one 10 kV for the amplifier. These high voltage power supplies charge internal capacitors to a preset voltage prior to laser firing. When the laser is fired, each capacitor is discharged into its respective flashlamp. The subsequent optical pulse from the flashlamps pumps the Nd:glass rods used for lasing. Concomitant with the discharging capacitors is a high frequency electromagnetic pulse that is easily detected by the dianostics used. Each individual piece of the experimental apparatus was constructed with internal shielding by the manufacturer and standard, shielded, coaxial cables were used for connections between all equipment. Despite these precautions, the electromagnetic noise pulse generated by the power supplies was sufficient to mask all essential information displayed on the oscilloscope. To further aggravate this problem, metal holders and stands on the optical bench, that were employed to hold various optical filters in front of the PIN SPOT/2D detector, acted as antennas and re-radiated small amounts of the electromagnetic noise. These secondary antennas complicated the problem of noise source isolation.

Several methods were used to reduce the electromagnetic noise from the laser power supplies. The first step taken was to isolate the diagnostic equipment, particularly the storage oscilloscope, from the 110 volt A.C. supply line in the laboratory. This was accomplished by placing an isolation transformer between the wall socket supply line and the power cord of the oscilloscope. Another noise reduction method was to remove all ground loops that were directly or indirectly connected to the vertical amplifier of the oscilloscope. A previous arrangement of the experimental apparatus incorporated a power supply for the PIN SPOT/2D detector that required a 110 volt source. This setup contained a ground loop from the detector power supply cord through the vertical amplifier to the oscilloscope power supply line. Since the detector power supply and the oscilloscope had a common connection through the wall socket, an inherent ground loop was formed. To eliminate this problem, the detector power supply was replaced by a shielded battery voltage supply attached directly to the rear of the detector as shown in Figure 20. This eliminated the common ground between the oscilloscope and detector. Since electromagnetic wave intensity is a function of $1/R^2$, where R is the distance from the source, one of the more simple methods of noise reduction involved moving the diagnostic equipment away from the EM noise

source. The confines of the laboratory limited this separation to approximately six meters, but this action aided considerably the noise reduction process. Another advantageous procedure was double shielding the coaxial cables between the detector and the oscilloscope, which decreased the EM noise picked up by standard BNC cables.

The 7A24 dual trace vertical amplifier unit of the storage oscilloscope has a summing capability that allows algebraic addition or subtraction of two input signals. To take advantage of the common-mode rejection capabilities offered, two coaxial cables were placed in the same double shielding jacket and connected between the oscilloscope and the PIN detector. As Figure 20 shows, a dummy BNC connector was mounted on the detector package. This was connected to channel one of the 7A24 by one of the coaxial cables in the common jacket. The second cable joined the PIN detector output with channel two of the 7A24. By inverting the channel two input signal to the 7A24 and summing it with the channel one signal, any common EM noise picked up by the two coaxial cables was eliminated. As well as reducing EM noise, this setup allowed a "positive" oscilloscope display. In other words, an increase in detector signal, which accompanies an increase in reflectivity of the silicon sample, produces a greater negative output voltage from the detector. This signal is inverted at the channel two input

of the 7A24 before it is displayed, so an increase in signal level on the oscilloscope display is indicative of an increase in sample reflectivity.

A final step taken to reduce the electromagnetic noise that appeared in the output display involved removing the metal, optical bench holders that were in close proximity of the PIN SPOT/2D detector. A metal shield mounted directly on the detector front was used instead of an optical bench stand to hold the optical bandpass filter. This eliminated the problem of re-radiation by secondary antennas.

The second classification of noise that masked or inhibited the output display of this experiment was optical. Once again, the source of this noise was the K-1500 laser system. White light from the flashlamps of both the laser oscillator and amplifier had sufficient intensity to flood the PIN SPOT/2D detector thereby concealing the important information displayed on the oscilloscope. This occurred even though the detector was facing away from the laser assembly. To remedy this situation optical shielding was used to cover the laser assembly and a five foot long hollow cardboard tube was placed at the output end of the laser amplifier along the beam axis. The inside of the cardboard tube was darkened with flat black paint. This ensured that most of the white light leakage from the flashlamps was

contained. However, even though these measures were taken, sufficient light travelled down the beam axis through the darkened tube to mask the TRR information. By employing a bandpass filter on the face of the PIN SPOT/2D detector, this final amount of optical noise was reduced to an acceptable level. The one nanometer wide bandpass filter was centered on the HeNe laser wavelength, 632.8 μm. A similar filter was utilized for the Argon Ion probe laser, with one nanometer bandpass centered at 488 μm.

Figures 26 and 27 show the sequence of noise shots taken prior to each data run. The first is the oscilloscope display with the PIN detector masked. All other equipment was configured for a normal test shot. The figure shows a few millivolts of high frequency electromagnetic noise. The latter is a picture of the oscilloscope display with the detector unmasked and the probe beam off. The difference between these two pictures is due to optical noise. Figure 28 is a noise shot taken with the bandpass filter removed. The large D.C. component of this signal is produced by the fraction of white light from the flashlamps traveling down the beam axis, and reflecting off the target into the PIN detector.

The noise reduction techniques outlined here enabled the discrimination of PIN SPOT/2D detector signal from the increased noise level attendant with the pulsed laser

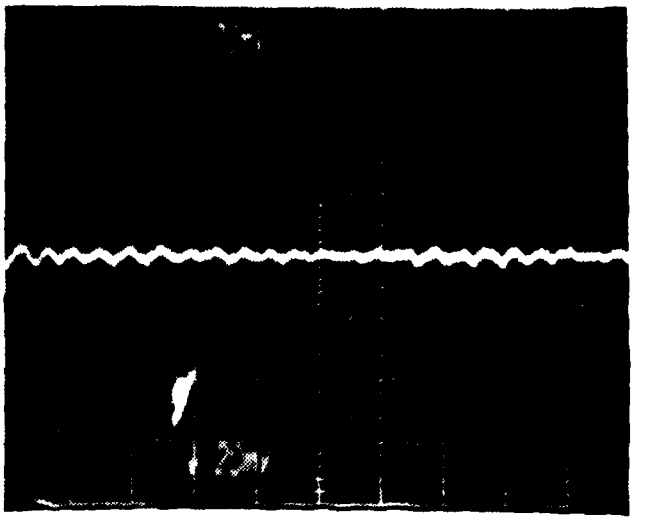

Figure 26. Output Signal of PIN Detector Showing High Frequency EM Noise

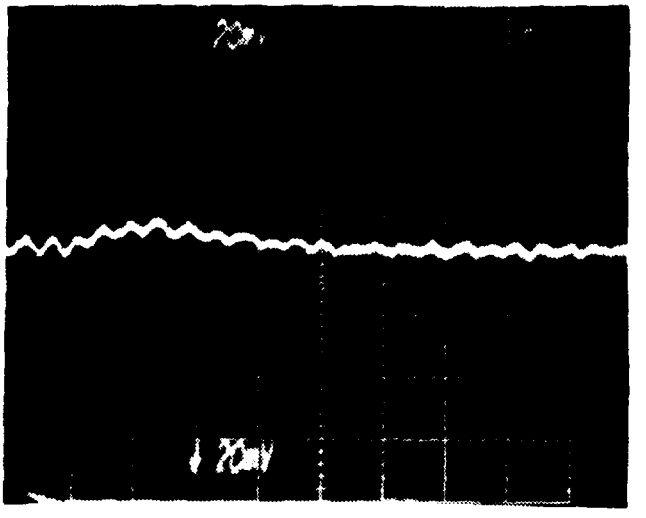

Figure 27. Output Signal of PIN Detector Showing High Frequency EM and Optical Noise

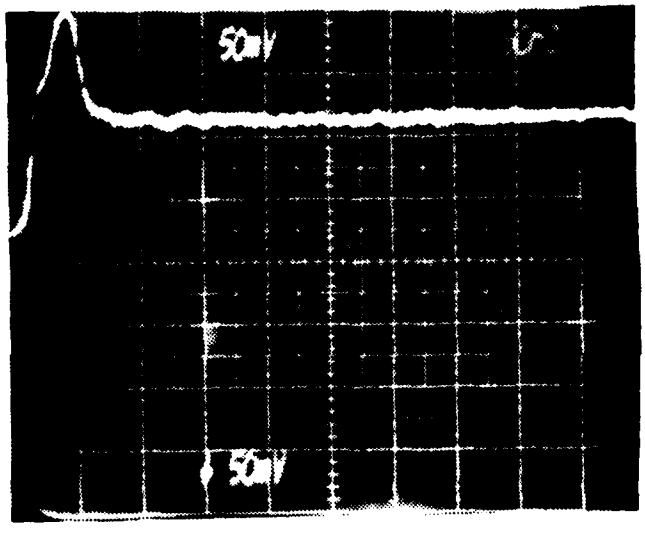

Figure 28. Output Signal of PIN Detector When Bandpass Filter is Absent

firing. It is hoped that future researchers may find these procedures useful when operating under similar constraints of signal to noise level or pulsed laser generated noise environments.

V. RESULTS

A. ANALYSIS OF TRR SIGNATURES

The results of the TRR experimentation were in general agreement with the empirical model of Lowndes et. al which was discussed previously (see Figure 6). Variances in τ_r, the time required for the reflectivity to rise from the D.C. value to the maximum value, were observed for the two different probe lasers. The Argon-Ion laser consistently exhibited longer rise times, a fact attributed to the spatial averaging effect of this laser's larger spot size (2 mm diameter vice the 1 mm diameter of the HeNe probe laser). The rise time for the HeNe laser was generally on the order of 30-40 ns as compared to the values of τ_r from 50-70 ns for the Argon-Ion laser. These figures were relatively constant for the respective probe beams at varying levels of pulsed laser energy density.

The total time for which the surface of the sample is molten is denoted by the symbol τ. Figure 29 shows the plot of τ versus pulsed laser energy density. The graph displays the observed result that τ increases for increasing values of energy density. As the energy density is increased, the melt front penetrates more deeply into the sample. After the heating laser pulse, the material begins to cool and

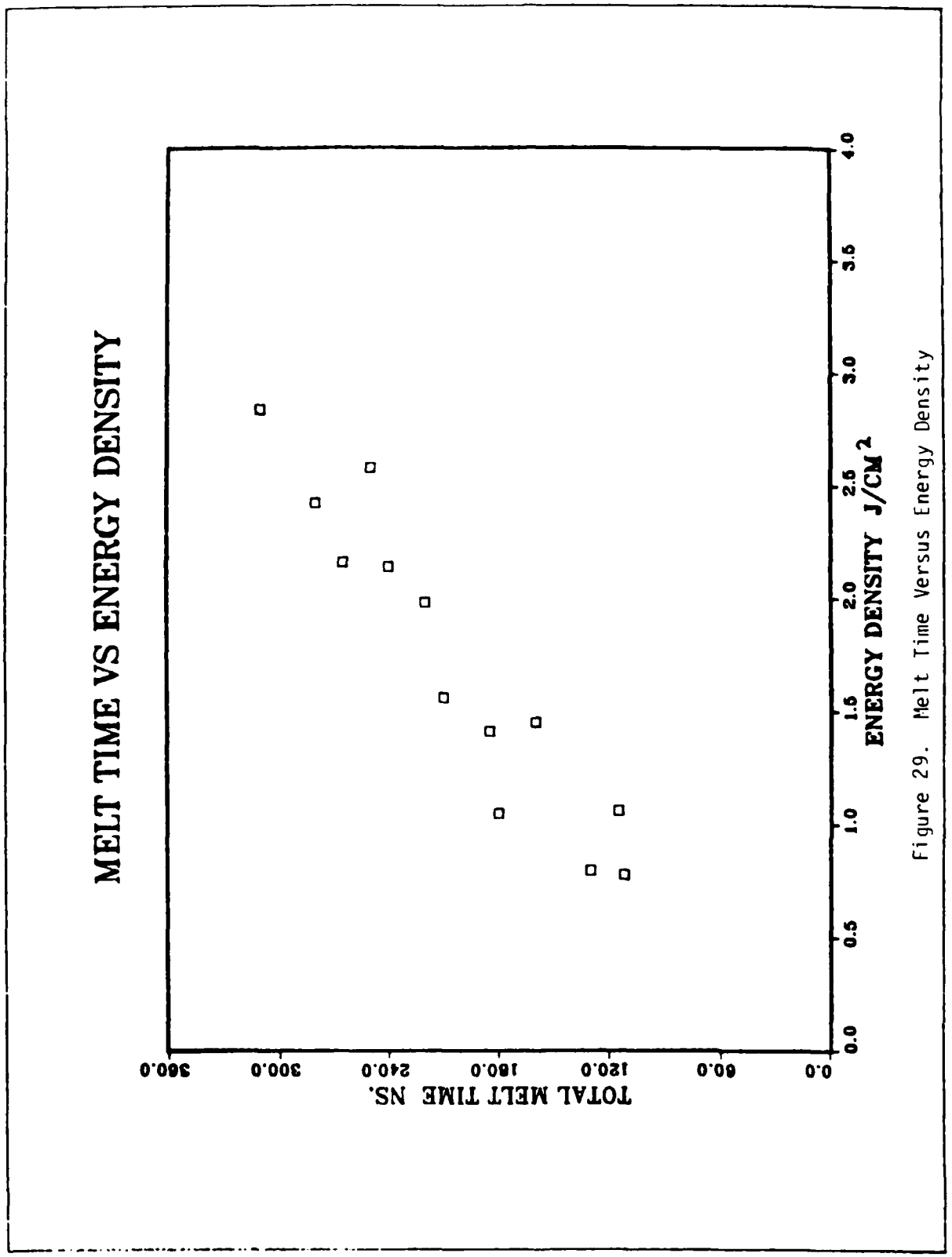

Figure 29. Melt Time Versus Energy Density

recrystallizes. Thus it can be seen qualitatively that the time required for complete recrystallization is dependent upon the depth to which the melt front has penetrated and consequently the energy density of the heating pulse.

The maximum value of reflectivity observed was dependent upon the pulsed laser energy density and the wavelength of the probe laser. Variations in the value of R(max)/R(DC), the normalized maximum reflectivity, for the different probe beams at similar pulsed laser energy densities were ascribed to differences in detector response for the two wavelengths (see Figure 18), the Si sample's reflectivity versus wavelength characteristics (Figure 12), and the dissimilarities in spot size and output power of the two probe lasers. The data, obtained utilizing the He-Ne probe and displayed in Figure 30, seem to approach an asymptotic value of normalized maximum reflectivity at R(max)/R(DC) equal to approximately 1.85. Using this number and the R(DC) value of 0.40 for the wavelength 632.8 nm, obtained from the Perkin-Elmer spectrophotometer, the actual value of peak reflectivity can be calculated. This calculation assumes linear detector response and that the reflectance standard used for the spectrophotometer (aluminized mirror) has an R value of 1.0 at 632.8 nm. With these assumptions the calculated value of R(max) was found to be 0.74, in good agreement with the accepted value for molten Si of 0.73

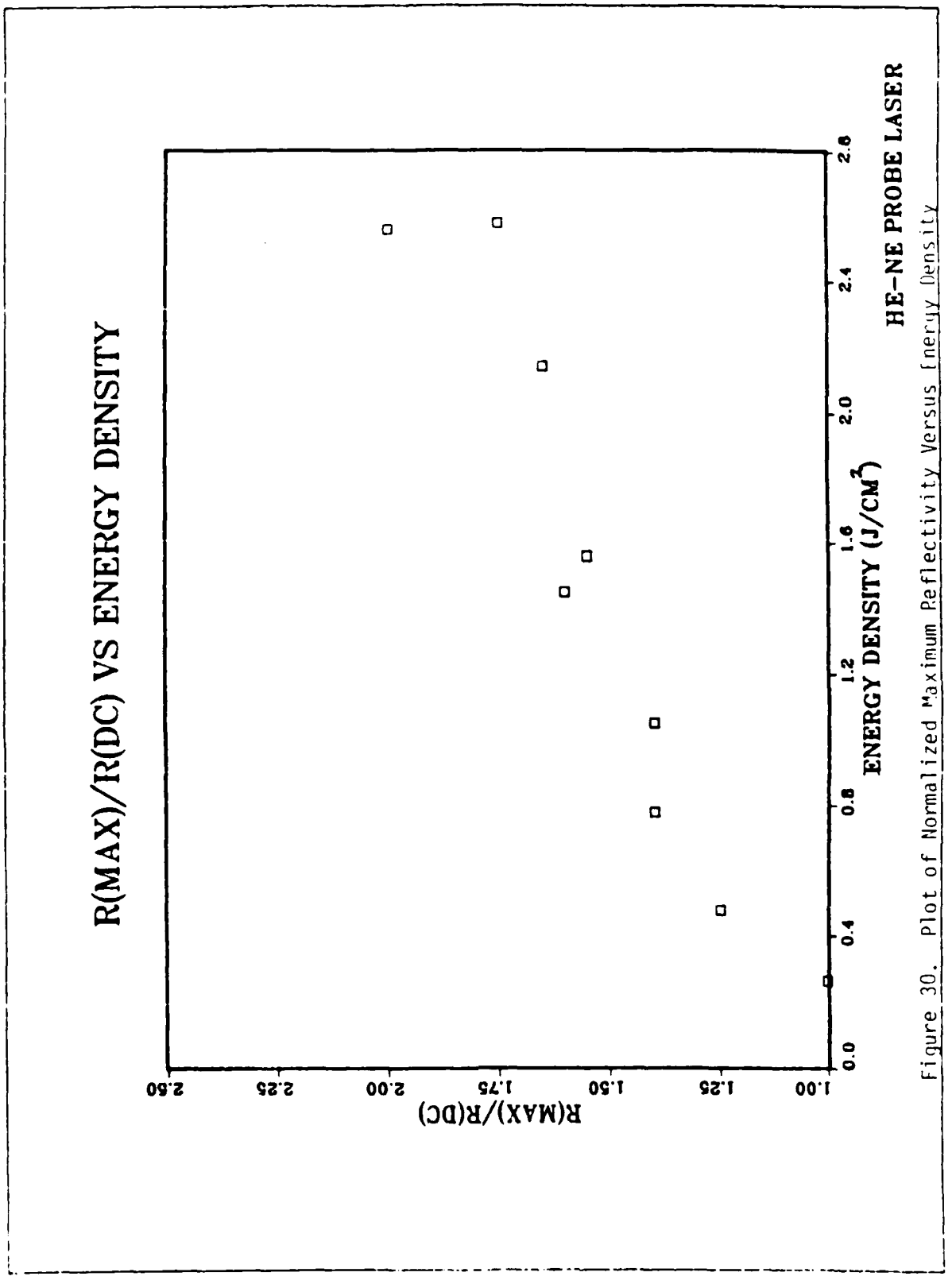

Figure 30. Plot of Normalized Maximum Reflectivity Versus Energy Density

[Ref. 37]. Unfortunately, no such calculation was possible utilizing the Argon-Ion probe laser data. No asymptotic limit was inferred from this data; R(max)/R(DC) continued to rise as pulsed laser energy density increased (see Figure 31). This was a peculiar finding as one would expect the maximum reflectivity to reach some constant value associated with molten Si, as was the case for the HeNe probe beam. The cause of this anomalous behavior may lie with errors in the spatial coincidence of the large Argon-Ion probe spot and the pulsed laser spot.

The threshold energy density for reflectivity increase for both probe beams was observed to be approximately 0.46 J/cm^2. Below this value of pulsed laser energy density, no evidence of enhanced reflectivity could be detected. For values of energy density from 0.46 to 1.05 J/cm^2 reflectivity from the surface showed an increase and following the laser pulse, a decrease to the original value of reflectivity, R(DC). Energy densities greater than 1.05 J/cm^2 produced enhanced reflectivity but also evaporated material from the target surface. This resulted in bulk surface damage and a final value of reflectivity less than R(DC). The degree to which the post-irradiated value of reflectivity was less than R(DC) was found to be dependent primarily upon energy density. Higher laser energy densities caused a greater level of material evaporation and

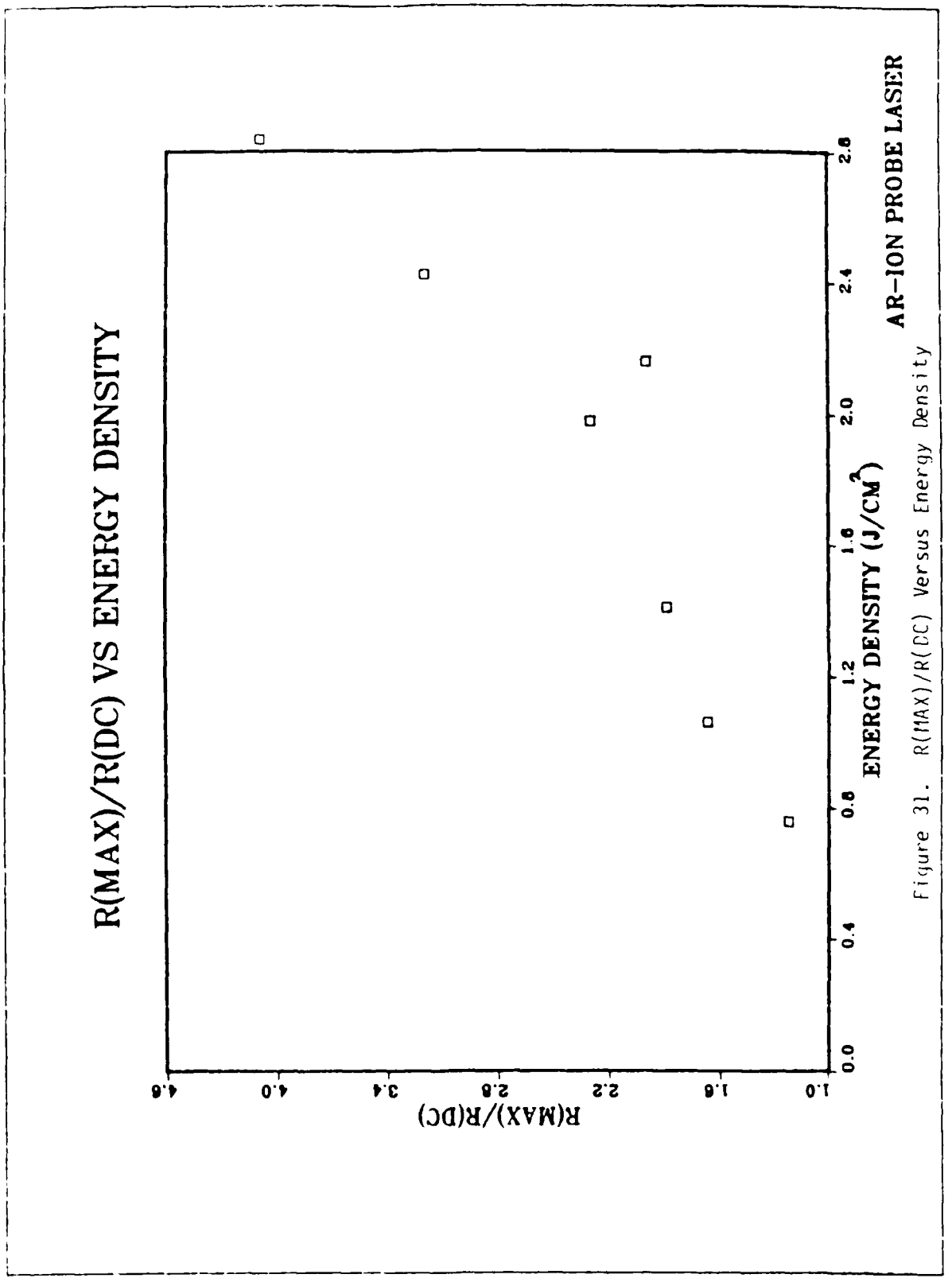

Figure 31. R(MAX)/R(DC) Versus Energy Density

cratering thereby roughening the sample surface and giving rise to less specular and more diffuse reflection of the probe beam. Figure 32 shows TRR signatures for various energy densities and from this depiction the value of these traces in the determination of thresholds for melting and bulk surface damage can be readily seen.

B. EXAMINATION OF SURFACE DAMAGE BY OPTICAL MICROSCOPY

Employment of optical microscopy to determine the energy density for surface damage to the target served to verify and refine the threshold value obtained by TRR measurements. Evidence of cratering in wafer surface was observed for laser energy densities greater than 0.88 J/cm^2. An optical micrograph of this damage level is displayed in Figure 33. The degree of surface irregularity caused by this energy density was insufficient to effect any major increase in the diffuse reflection component of the probe laser beam. Figures 34 through 37 show an increasing extent of surface cratering for corresponding increases in pulsed laser energy density. In addition, these figures demonstrated that the crater density decreases with distance from the center of the laser pulse impact area. This was to be expected as the laser pulse was best described as Gaussian in shape.

Correlation of the optical micrographs with the TRR signatures showed the threshold for surface damage was between 0.88 and 1.05 J/cm^2, and the dependence of the

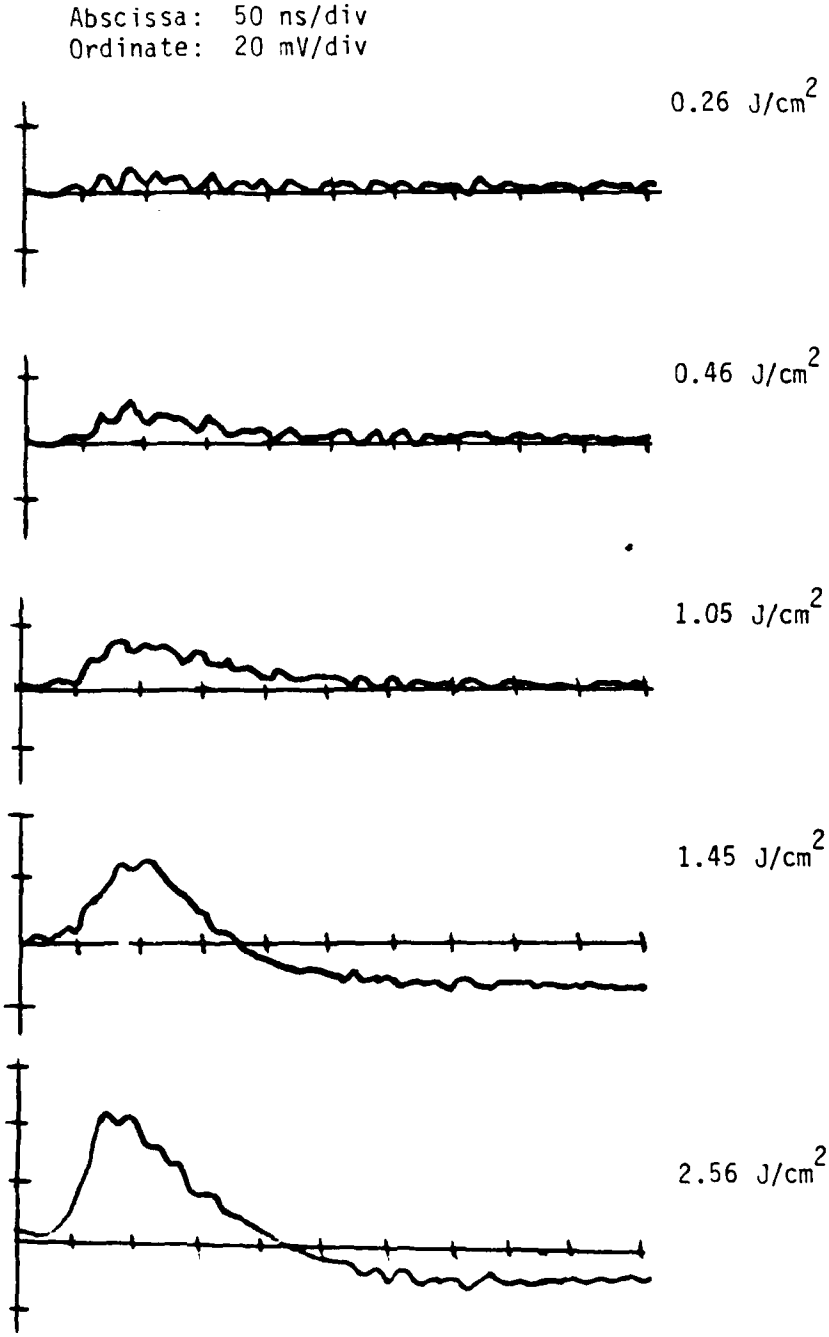

Figure 32. TRR Signatures of Si(100). Nd:glass Laser Heating Pulse (1.06 μm), HeNe cw Probe Laser (632.8 nm)

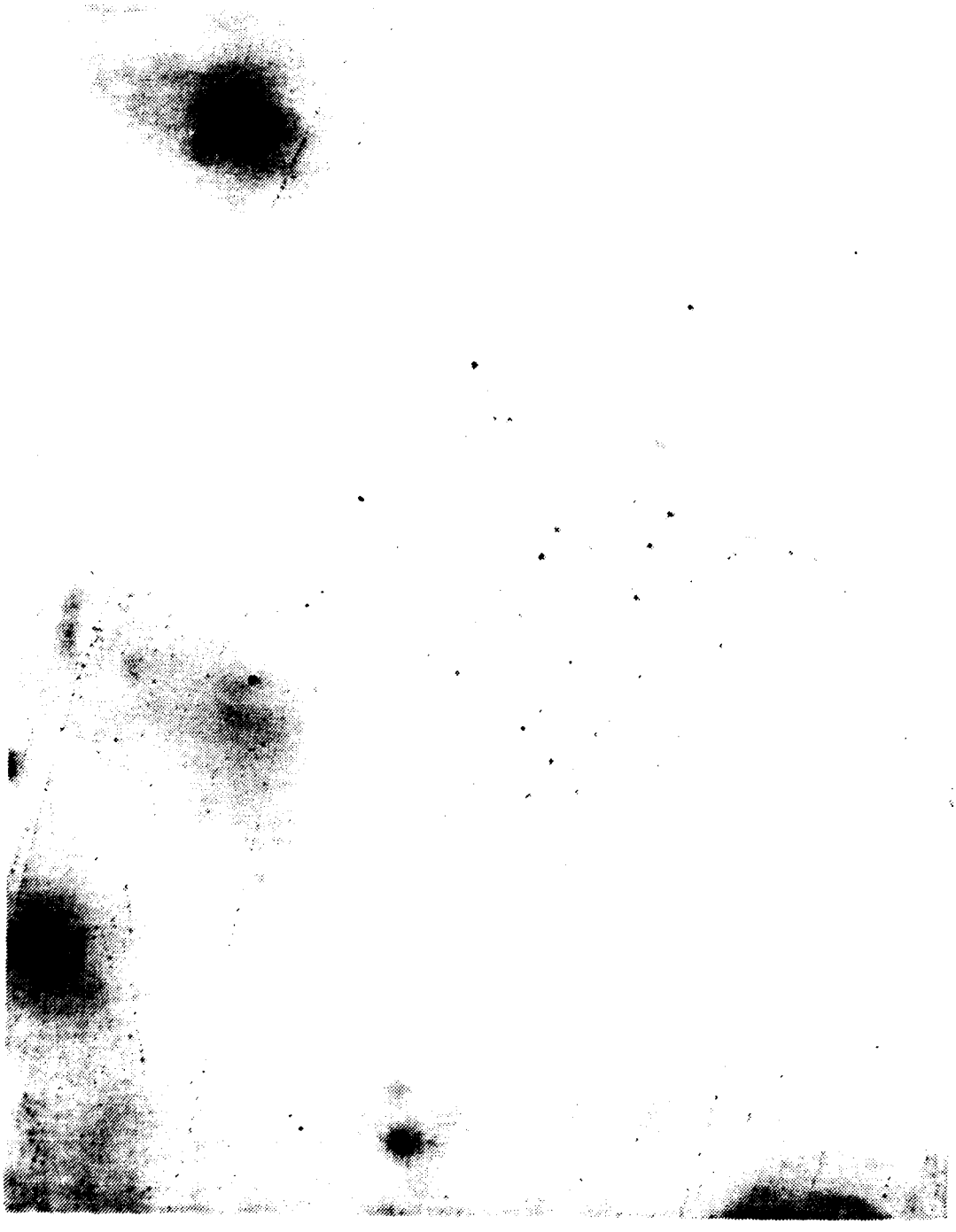

Figure 33. Laser-Induced Surface Damage to Si Wafer at a Laser Energy Density of 0.88 J/cm^2
(100X magnification by optical microscope)

Figure 34. Laser-Induced Surface Damage to Si Wafer, at a Laser Energy Density of 1.21 J/cm^2
(50X magnification by optical microscope)

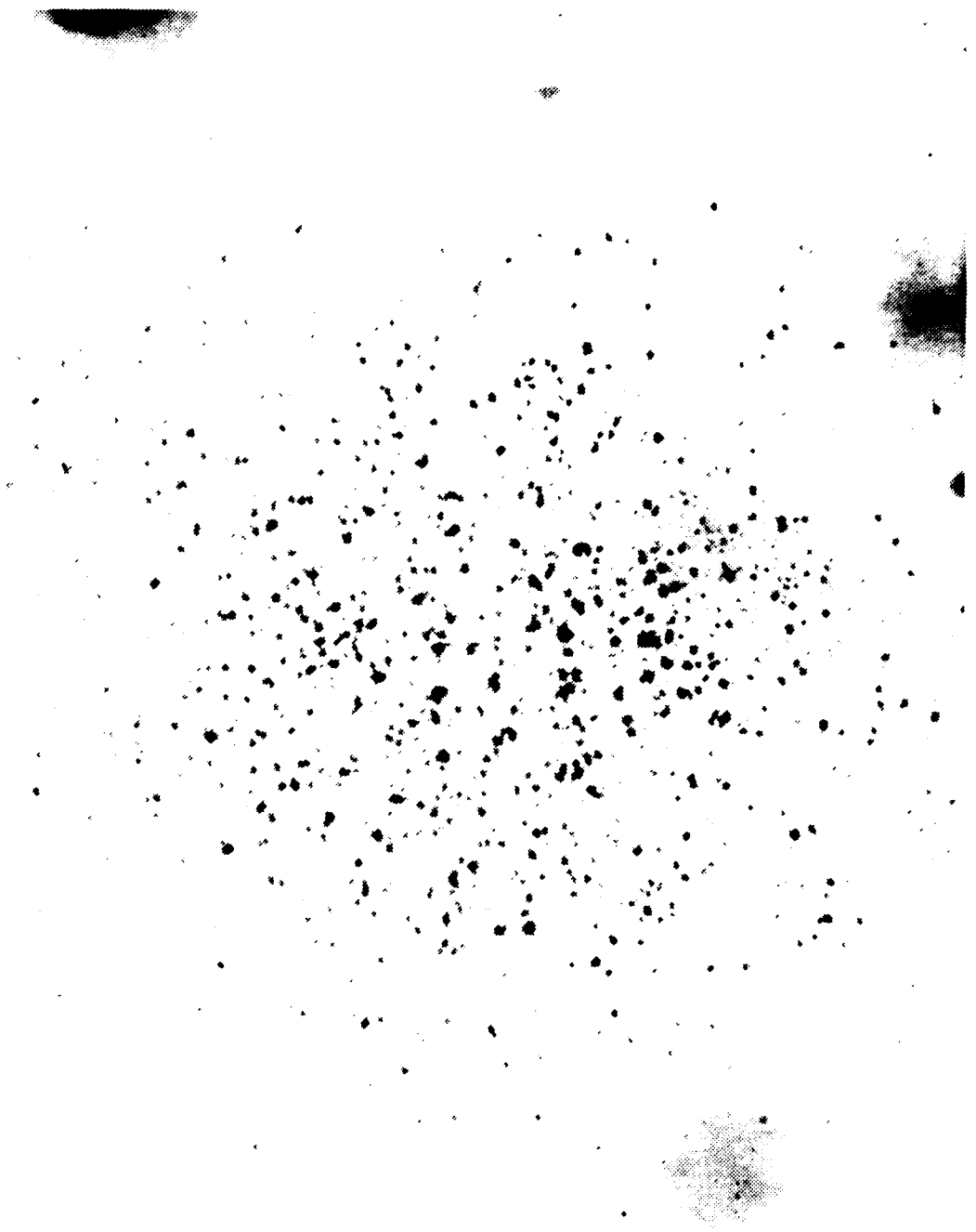

Figure 35. Laser-Induced Surface Damage to Si Wafer, at a Laser Energy Density of 1.47 J/cm^2
(50X magnification by optical microscope)

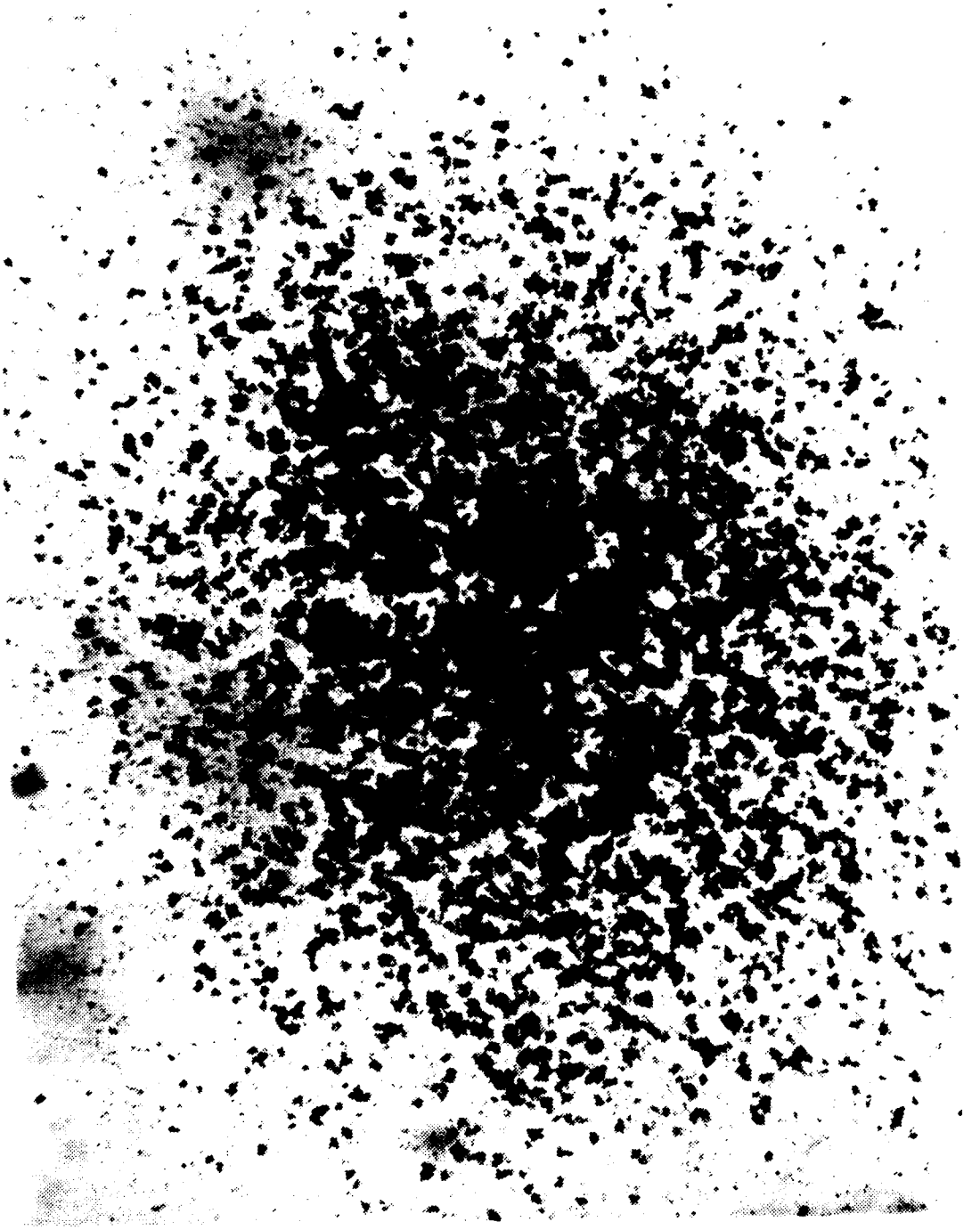

Figure 36. Laser-Induced Surface Damage to Si Wafer, at a Laser Energy Density of 2.56 J/cm^2
(50X magnification by optical microscope)

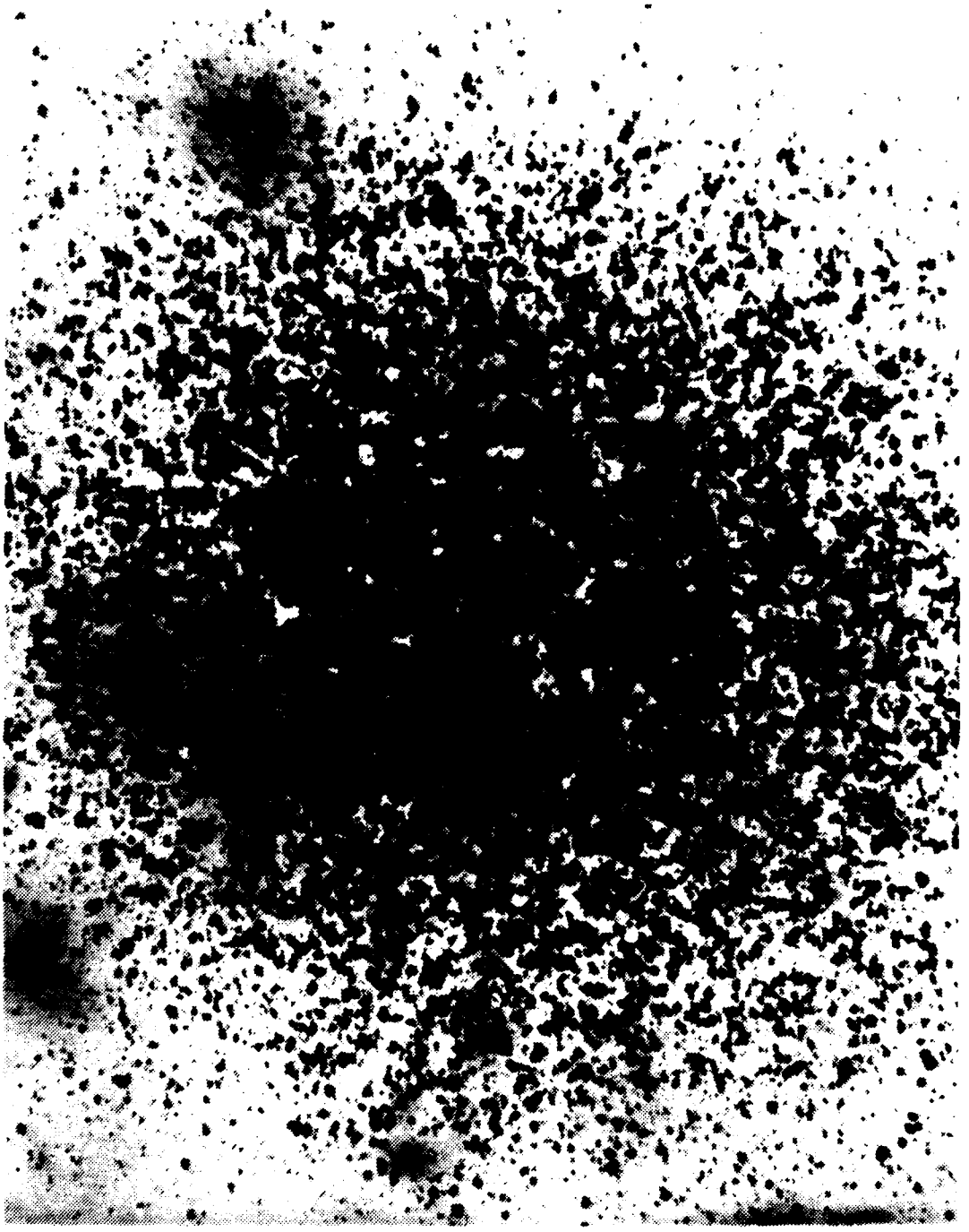

Figure 37. Laser-Induced Surface Damage to Si Wafer, Energy Density on Target, 3.3 J/cm^2
(50X magnification by optical microscope)

severity of surface damage upon pulsed laser energy density was confirmed.

C. SPECULAR VERSUS DIFFUSE REFLECTION

It was found that surface damage due to laser pulses with energy densities of less than ≈ 1.2 J/cm^2 contributed little to the formation of a diffuse component of reflection. Increases in the diffuse component were noted when the TRR traces showed a value of R(final) less than the original R(DC). The primary mechanism for this change from specular reflection was laser-induced surface damage. Figure 38 displays this fundamental concept. The results of specular versus diffuse reflection measurements for an undamaged sample and an irradiated sample are shown in Figure 39. Further work on quantitative measurements of the variation between specular and diffuse reflection for varying laser energy densities would be of significant interest to military applications of lasers as EO countermeasures.

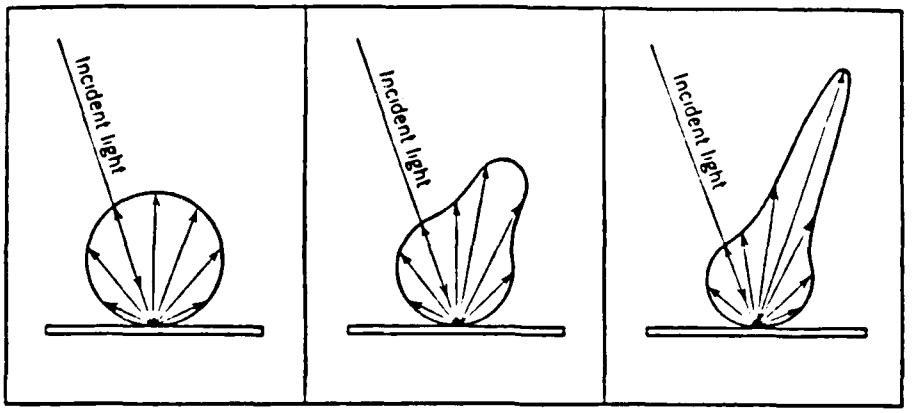

Figure 38. Polar Diagrams Showing the Reflection Obtained from Surfaces of Decreasing Roughness

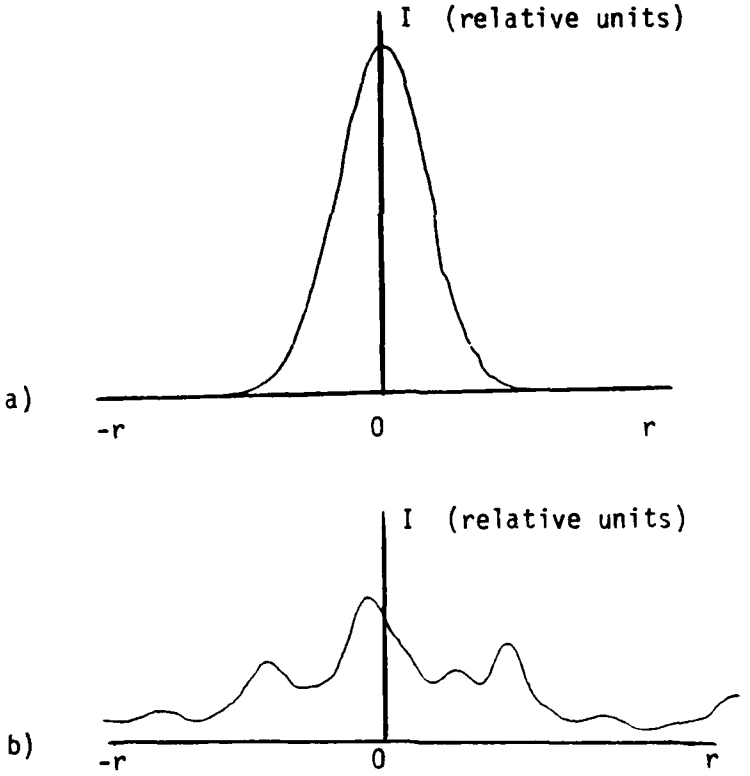

Figure 39. Probe Laser Irradiance Versus Beam Radius for Reflection from Si Sample: a) before irradiation, b) after 3.3 J/cm^{-2}, 20 ns pulse

VI. CONCLUSIONS

Time-resolved reflectivity measurements during pulsed Nd:glass laser irradiation of extrinsic silicon were performed to determine the energy density thresholds for melting and surface damage. Studies using optical microscopy (50 X) were conducted to verify the extent of surface damage to the irradiated semiconductor samples. Qualitative correlation between the laser-induced surface damage and the degree of probe laser beam scattering was also conducted.

TRR proved to be an accurate indicator of surface melting due to pulsed laser optical heating. The duration of the solid to liquid phase change was easily ascertained by employing the TRR technique. It was found that the duration of surface melting for the p-type silicon was proportional to the incident laser pulse energy density. The threshold or minimum value of energy density to accomplish surface melting was observed to be approximately 0.4 J/cm^2. Surface damage of a magnitude to cause significant scattering of the probe laser beam occurred for incident energy density values of 1.05 J/cm^2 or greater. This was verified by the optical microscopy studies. The surface damage was caused by evaporation of target material due to the higher pulsed laser fluences.

Several experimental factors, in addition to pulsed laser energy density, affected the nature of the TRR signatures. A dependency of the reflectivity rise and fall times upon probe laser beam spot size was noted. Larger spot size caused lengthened rise and fall times due to spatial averaging effects. Perhaps the most important single factor was the choice of detector. The PIN SPOT/2D served adequately in this experimentation, displaying sufficient sensitivity and response time for operation in the nanosecond time regime. Other locally-held detectors, including the Lasermetrics and KORAD K-1, were deemed unsatisfactory for this application.

In summary, TRR provided information concerning target damage which was unobtainable through post-irradiation measurements. The nanosecond time scale resolution of the laser-induced damage process allowed for accurate analysis of the target melt dynamics.

VII. RECOMMENDATIONS FOR FURTHER RESEARCH

The study of laser effects upon semiconductors involves the investigation of a multitude of physical phenomena. This research has dealt with but one of these areas of interest, time-resolved reflectivity. During the course of this experimentation, topics of possible importance with regard to future research became evident.

Thresholds of laser energy density for the melting and surface damage of other semiconductor materials may be determined using the TRR technique. Gallium arsenide and mercury-cadmium telluride are but two of the technologically significant substances which would be likely choices as target material. The apparatus described herein is, in fact, suitable for measuring the TRR of any highly-polished (i.e., specularly reflecting) surface. The target need not be a semiconductor, as perhaps results of multi-layer dielectric reflection under the influence of pulsed laser irradiation might be of some import. Ultimately, it would be desirable to irradiate actual photodetectors and EO sensors so as to ascertain their susceptibility to laser damage.

The versatility and usefulness of the Nd:glass pulsed laser system could be improved through eventual modifications. The implementation of a beam homogenizer, effecting

a uniform cross-sectional beam energy density, would allow more accurate spatial determination of energy deposition on the target. In addition, the use of a KDP (potassium dihydrogen phosphate) crystal to accomplish efficient frequency doubling would enable the laser system to produce Q-switched, giant pulses in the visible range of the spectrum. For the annealing of semiconductors, the visible pulse would provide a more efficient laser energy-target coupling.

Increasing the range of laser energy densities to values greater than three Joules per cm^2 would be a logical extension of this research. However, at sufficiently high energy densities dielectric breakdown of air and plasma production occur. For this reason high energy density studies should be conducted in vacuo. Solid-state as well as electrical analysis of the irradiated samples remains to be investigated. Variations in extrinsic semiconductor impurity concentrations and electrical conductance and the possible deletericus effects of such variations on detector performance may warrant future examination.

Finally, the concept of specular versus diffuse reflection from the laser irradiated silicon wafer was only qualitatively pursued in this research. Further efforts to quantitatively measure the specular versus diffuse components of reflectivity, following the semiconductor's

irradiation by varying laser energy densities, would be worthwhile and have considerable bearing on the subject of EO countermeasures.

AD-A150 350 TIME-RESOLVED REFLECTIVITY MEASUREMENT OF EXTRINSIC SILICON DURING PULSED LASER IRRADIATION(U) NAVAL POSTGRADUATE SCHOOL MONTEREY CA G D JOHNSON ET AL. 2/2

UNCLASSIFIED JUN 84 F/G 20/6 NL

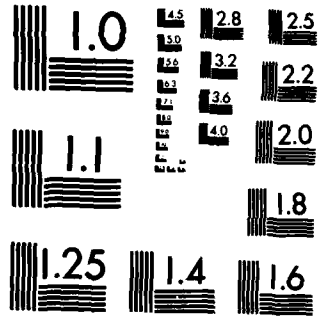

MICROCOPY RESOLUTION TEST CHART
NATIONAL BUREAU OF STANDARDS-1963-A

LIST OF REFERENCES

1. Jane's Weapons Systems, 1983-84, pp. 707-806, McGraw-Hill, 1983.

2. Musa, S., "Science and Technology Perspectives for Electro-Optical Warfare," Journal of Electronic Defense, pp. 25-26, January 1983.

3. Radio Corporation of America, Electro-Optics Handbook, 2nd ed., p. 146, RCA, 19.

4. Kittel, C., Introduction to Solid State Physics, Chapter 13, John Wiley, 1956.

5. Verdeyen, J.T., Laser Electronics, Chapter 14, Prentice-Hall, 1981.

6. Yariv, Amnon, Introduction to Optical Electronics, Chapter 11, Holt, Rinehart, and Winston, 1976.

7. Verdeyen, J.T., p. 392.

8. Sclar, N., "Extrinsic Silicon Detectors for 3-5 and 8-15 μm," Infrared Physics, v. 16, pp. 435-448, 1976.

9. Steckl, A.J., "Extrinsic Silicon Characteristics," The Infrared Handbook, W.C. Wolfe and G.J. Zissis, eds., p. 11-88, Office of Naval Research, 1978.

10. Slawek, J.E., Jr., The Photovoltaic Indium Antimonide Infrared Detector, pp. 8-9, Barnes Engineering Company, 1971.

11. O'Shea, D.C., et. al., Introduction to Lasers and Their Applications, pp. 227-228, Addison-Wesley, 1978.

12. RCA Electro-Optics Handbook, p. 181.

13. The Infrared Handbook, p. 13-24.

14. Lowrance, J.L., "A Review of Solid State Image Sensors," Advances in Electronics and Electron Physics, Morgan and McMullan, eds., pp. 421-424, 1979.

15. Shepherd, F.D., "Schottky IRCCD Thermal Imaging," Advances in Electronics and Electron Physics, Morgan and McMullan, eds., pp. 495-512, 1979.

16. Shapiro, J.L., ed., Modern Utilization of Infrared Technology, v. 124, Proceedings of the Society of Photo-Optical Instrumentation Engineers, 1977.

17. Chan, W.S., eds., Advances in Focal Plane Technology, v. 217, Proceedings of the Society of Photo-Optical Instrumentation Engineers, 1980.

18. Krikorian, E., ed., Infrared Image Sensor Technology, v. 225, Proceedings of the Society of Photo-Optical Instrumentation Engineers, 1980.

19. Grinberg, A.A., et. al., "Absorption of Laser Radiation and Damage in Semiconductors," Soviet Physics Solid State, v. 9, pp. 1085-1090, November 1967.

20. Meyer, J.R., et al., "Optical Heating in Semiconductors: Laser Damage in Ge, Si, InSb, and GaAs," Journal of Applied Physics, v. 51, pp. 5513-5521, October 1980.

21. Bairi, P., et. al., "A Melting Model for Pulsing Laser Annealing of Implanted Semiconductors," Journal of Applied Physics, v. 50, pp. 788-796, February 1979.

22. Rimini, E., et. al., "Ruby Laser Pulse Effects in Ion Impanted Semiconductors," Laser-Solid Interactions and Laser Processing--1978, Ferris et. al., ed., pp. 259-273, American Institute of Physics, 1978.

23. Auston, D.H., et. al., "Dynamics of Laser Annealing," op. cit., pp. 11-26.

24. Bartoli, F., et. al., "Irreversible Laser Damage in IR Detector Materials," Applied Optics, v. 16, pp. 2934-2936, November 1977.

25. Van Vechten, J.A., "The Gentle Electronic Nature of Pulsed Beam Annealing, or Does It Really Go Superfluid?," Laser and Electron Beam Interactions with Solids, B.R. Appleton and G.K. Cellar, eds., pp. 49-60, Elsevier Science, 1981.

26. Bartoli, F., et. al., "The Thermal Recovery Processes in Laser Irradiated HgCdTe (PC) Detectors," Applied Optics, v. 14, pp. 2499-2501, October 1975.

27. Giuliani, J.F., Marquardt, C.L., "Electrical Effects in Laser-Damaged Phototransistors," Journal of Applied Physics, v. 45, no. 11, November 1974.

28. Lowndes, D.H., and Wood, R.F., "Time-Resolved Reflectivity During Pulsed Laser Annealing of GaAs," Applied Physics Letters, v. 38, pp. 971-973, 15 June 1981.

29. Pospieszczyk, A., et. al., "Pulsed Laser Annealing of GaAs and Si: Combined Reflectivity and Time-of-Flight Measurements," Journal of Applied Physics, v. 54, pp. 3176-3182, June 1983.

30. Galvin, J., et. al., "Time-Resolved Conductance and Reflectance Measurements of Silicon During Pulsed-Laser Annealing," Physics Review B, v. 27, pp. 1079-1087, 15 January 1983.

31. Takai, M., et. al., "Dynamic Behavior of Nanosecond Pulsed Nd:Glass Laser Annealing in Ion Implanted Silicon," Laser and Electron Beam Interactions with Solids, Appleton and Cellar, eds., pp. 91-96, Elsevier Science, 1981.

32. Murakami, K., et. al., "Dynamic Behavior of Pulsed-Laser Annealing in Ion-Implanted Silicon: Measurement of the Time Dependent Optical Reflectance," Physics Letters, v. 70A, pp. 332-334, 19 March 1979.

33. White, C.W., et. al., "Laser Annealing of Ion-Implanted Silicon," Laser-Solid Interactions and Laser Processing--1978, Ferris et. al., eds., pp. 275-290, American Institute of Physics, 1979.

34. Davis, L.J., Self-Generated Magnetic Fields Produced by Laser Bombardment of a Solid Target, Masters Thesis, Naval Postgraduate School, Monterey, California, 1972.

35. Cullis, A.G., et. al., "A Device for Laser Beam Diffusion and Homogenization," Journal of Physics E: Scientific Instrumentation, v. 12, 1979.

36. Interviews with Distinguished Professor of Physics, E. Crittenden, Monterey, California, March 1984.

37. Shvarev, B.A., et. al., "Optical Properties of Liquid Silicon," Soviet Physics Solid State, v. 16, p. 2111, 1975.

INITIAL DISTRIBUTION LIST

		No. Copies
1.	Defense Technical Information Center Cameron Station Alexandria, Virginia 22314	2
2.	Library, Code 0142 Naval Postgraduate School Monterey, California 93943	2
3.	Department Chairman, Code 61 Department of Physics Naval Postgraduate School Monterey, California 93943	2
4.	Professor A. W. Cooper, Code 61Cr Department of Physics Naval Postgraduate School Monterey, California 93943	3
5.	Professor S. Garrett, Code 61Gx Department of Physics Naval Postgraduate School Monterey, California 93943	1
6.	Professor F. Schwirzke, Code 61Sw Department of Physics Naval Postgraduate School Monterey, California 93943	1
7.	LT Emory L. Chenoweth, USN 1119 Isabella Court Coronado, California 92118	2
8.	LT Geoffrey D. Johnson, USN 87 Stoughton Road Dedham, Massachusetts 02026	2

END

FILMED

3-85

DTIC